

# Validation and assessment of satellite-based columnar CO<sub>2</sub> and CH<sub>4</sub> mixing-ratios from GOSAT and OCO-2 satellites over India

Harish Gadhavi<sup>1</sup>, Akanksha Arora<sup>1,2</sup>, Chaithanya Jain<sup>3</sup>, Mahesh Kumar Sha<sup>4†</sup>, Frank Hase<sup>5</sup>, Matthias Frey<sup>6†</sup>, Srikanthan Ramachandran<sup>1</sup>, Achuthan Jayaraman<sup>3</sup>

<sup>1</sup>Space and Atmospheric Science Division, Physical Research Laboratory, Ahmedabad, India

<sup>2</sup>Indian Institute of Technology Gandhinagar, Gandhinagar, India

<sup>3</sup>National Atmospheric Research Laboratory, Gadanki, India

<sup>4</sup>Royal Belgian Institute for Space Aeronomy, Brussels, Belgium

<sup>5</sup>Institute of Meteorology and Climate Research, Karlsruhe Institute of Technology, Karlsruhe, Germany

<sup>6</sup>National Institute for Environmental Studies, Tsukuba, Japan

<sup>†</sup>Formerly at Institute of Meteorology and Climate Research, Karlsruhe Institute of Technology, Karlsruhe, Germany

Correspondence to: Harish Gadhavi ([hgadhavi@prl.res.in](mailto:hgadhavi@prl.res.in))

**Abstract.** ~~The OCO-2 and GOSAT series of satellites provide near-global coverage of CO<sub>2</sub> and CH<sub>4</sub> mixing-ratios. To accurately derive emission fluxes from the observed mixing ratios, it is crucial that these data meet specific precision and systematic error requirements. In this study, we report validation results for GOSAT and OCO-2 over South Asia, obtained using a portable Fourier Transform infrared Spectrometer (FTS) at a tropical rural site (Gadanki; Latitude: 13.45° N, Longitude: 79.18° E) in Southern India, from November 2015 to July 2016. Biases in CH<sub>4</sub> mixing ratios from GOSAT ranged from -9 to -18.5 ppb, depending on the collocation criteria, while CO<sub>2</sub> data from OCO-2 demonstrated better accuracy and precision, meeting the requirements of ESA's Climate Change Initiative (CCI). Using the FLEXPART model, we also show that CH<sub>4</sub> emissions from regional sources accounted for only 35% of the day-to-day observed variability. Both model-derived and observed mixing ratios exhibited the same seasonal variation, with higher values in October-November and lower values in June-July. However, the observed mixing ratios decreased by approximately 100 ppb, while the model-derived values decreased by only 20 ppb, suggesting that atmospheric chemistry and variations in background concentrations play a significant role over South India.~~

Satellite observations of column-averaged carbon dioxide (XCO<sub>2</sub>) and methane (XCH<sub>4</sub>) mixing-ratios provide essential data for monitoring greenhouse gas emissions. However, the accuracy of emission estimates depends on the precision and bias of satellite retrievals, which require validation against ground-based reference measurements. This study presents a systematic validation of XCO<sub>2</sub> and XCH<sub>4</sub> data from GOSAT and OCO-2 satellites over South India using ground-based Fourier Transform Spectrometer (FTS) observations at Gadanki (13.5°N, 79.2°E) collected during October 2015 to July 2016. Satellite products from National Institute for Environmental Studies, Japan (NIES), NASA's Atmospheric CO<sub>2</sub> Observations from Space (ACOS) project, USA (ACOS), and the University of Leicester, UK (UoL) were evaluated using a three-step spatial-temporal pairing method. Results show that the UoL's proxy XCH<sub>4</sub> product meets the European Space Agency's Climate Change Initiative (ESA CCI) bias requirement (<10 ppb) across all spatial windows, while the NIES XCH<sub>4</sub> product meets the requirement only for intermediate spatial scales. For XCO<sub>2</sub>, NASA ACOS and OCO-2 products meet the CCI bias requirement (<0.5 ppm), while NIES XCO<sub>2</sub> exceeds this threshold. All products satisfy the precision requirement (<8 ppm) with substantial margins. Additionally, FLEXPART model simulations using regional emission inventories revealed that agricultural activities dominate seasonal methane enhancements, contributing about 55%, followed by waste and wetland emissions. The model captured seasonal trends but underestimated the amplitude of observed variations, highlighting the influence of changing background methane levels. These findings demonstrate the

suitability of recent satellite products for regional greenhouse gas monitoring and emphasize the need for expanding ground-based FTS networks across South Asia to support improved emission assessments.

## 1 Introduction

Carbon dioxide (CO<sub>2</sub>) and methane (CH<sub>4</sub>) are the two top most important greenhouse gases (GHGs) responsible for anthropogenic global warming. While the role of CH<sub>4</sub> in global warming is of primary interest, CH<sub>4</sub> also plays an important role in atmospheric chemistry by affecting OH amount, ozone production in remote areas and water (production) in the stratosphere (Fiore et al., 2002; Fleming et al., 2015; Laughner et al., 2021; Noel et al., 2018). Both CO<sub>2</sub> and CH<sub>4</sub> abundances in the atmosphere are on continuous rise post-industrial era (Dunn et al., 2022; Turner et al., 2022) and hence a continuous global monitoring of carbon dioxide and methane is highly desirable for identifying sources, sinks, trends and effective implementation of global treaties on reduction of greenhouse gases by individual countries. Satellites due to their continuously improving data products, have come to be recognized as important tool in recent decade for monitoring and studying greenhouse gases. Satellites such as GOSAT ([Greenhouse gases Observing SATellite](#)) and OCO-2 ([Orbiting Carbon Observatory-2](#)) capture scattered solar radiation in the near infrared spectral region and provide columnar mixing ratios. GOSAT and OCO-2 are providing global coverage every 3 days and 15-16 days respectively (Table 1).

**Table 1. Launch date, equator crossing time, revisit time for global coverage and sensor technology of satellites, the data of which are used in the study.**

Name of satellite/sensor	Agency responsible for launch / maintenance	Launch Date	Equator crossing time	Satellite revisit time on same location	Greenhouse Gas related Data products	Principle of measurement
GOSAT aka Ibuki	JAXA, Japan / NIES, Japan	23 January 2009	13:00	3 days	Columnar CO <sub>2</sub> Columnar CH <sub>4</sub> CO <sub>2</sub> profile CH <sub>4</sub> profile	Fourier Transform Spectrometer
OCO-2 (Orbiting Carbon Observatory - 2)	JPL, USA	July 2014	13:35	16 days	Columnar CO <sub>2</sub>	Diffraction grating <a href="#">Spectrometer</a>

Satellite based estimates of greenhouse and trace gases have proved effective for deriving the emission fluxes (Bergamaschi et al., 2007, 2009; Bousquet et al., 2010; Chevallier et al., 2005). However, the improvement that can be achieved in emission fluxes depends highly on the accuracy of satellite retrievals. Climate Change Initiative (CCI) programme of European Space Agency (ESA) has listed the threshold precision and systematic error requirements for satellite derived columnar CO<sub>2</sub> and CH<sub>4</sub> mixing ratios (henceforth, columnar mixing ratios of CO<sub>2</sub> and CH<sub>4</sub> are represented by symbols XCO<sub>2</sub> and XCH<sub>4</sub> respectively), which are < 8 ppm precision and < 0.5 ppm systematic error for XCO<sub>2</sub> individual measurements, and < 34 ppb precision and < 10 ppb systematic error for XCH<sub>4</sub> individual measurements for deriving the regional emission fluxes of these species (Chevallier et al., 2016). WMO's Global Climate Observing System (GCOS) implementation plan has listed 1-sigma accuracy requirement of < 0.5 ppm for XCO<sub>2</sub> and < 5 ppb for XCH<sub>4</sub>, respectively (GCOS-200, 2016).

To validate satellite-based estimates, standards against which the satellite observations can be compared are needed. The Total Carbon Column Observing Network (TCCON) operates high-resolution ground-based Fourier transform infrared

spectrometers (FTS) for providing column-averaged greenhouse gas abundances with high accuracy and precision. TCCON observations serve as the reference data source for satellite validation. Recently, TCCON is supplemented by portable FTS operated in the framework of the Collaborative Carbon Column Observing Network (COCCON). TCCON currently operates more than 20 stations worldwide for high precision measurements of column average dry air mole fractions of CO<sub>2</sub>, CH<sub>4</sub>, N<sub>2</sub>O, HF, CO, H<sub>2</sub>O and HDO (<https://tccon-wiki.caltech.edu>; accessed in Sep 2024). All the sites follow common set of standards for instrumentation, data acquisition, calibration and analysis as prescribed by the TCCON Steering committee. TCCON sites use IFS 125HR FTS manufactured by Bruker Optics which cover a spectral range from 3900 cm<sup>-1</sup> to 15500 cm<sup>-1</sup> with a spectral resolution of 0.02 cm<sup>-1</sup>. The calibration of TCCON is achieved using aircraft profiling over the sites. ~~Typical~~ Errors in XCO<sub>2</sub> and XCH<sub>4</sub> are ~~is~~ less than 0.162% and 0.4% respectively for solar zenith angle less than 82.3° (Laughner et al., 2024; Wunch et al., 2011a). While the XCO<sub>2</sub> and XCH<sub>4</sub> measured at TCCON sites are highly accurate and very important for validation of satellite, model and other instruments, the spectrometer is expensive, large and requires continuous maintenance. The IFS 125HR FTS dimensions are of the order of 1 m x 1 m x 3 m and weighs several 100 kg, restricting its wide spread use or its deployment for short field campaigns or at remote sites with limited manpower. To supplement TCCON observations and to provide wider coverage of GHG observations, the Karlsruhe Institute of Technology (KIT) in collaboration with Bruker Optics, started developing a new type of portable FTS in 2011 which provides accurate measurement of GHGs while being lightweight and cost-effective. The prototype performance is described in Gisi et al. (2012). The spectrometer has become commercially available since 2014 under model designation EM27/SUN. Sha et al. (2020) compared the four different types of low-resolution spectrometers against IFS 125HR as well as in-situ observations using AirCore from one of the TCCON site over a period of 8 months and found EM27/SUN had the best performance matrix against high resolution spectrometer. COCCON is an emerging network of the portable FTS which uses tested and calibrated EM27/SUN spectrometers as well as common algorithms for data processing (Alberti et al., 2022a; Frey et al., 2019; Sha et al., 2020). Support for calibration and data processing is provided by KIT and the COCCON spectrometers are calibrated against TCCON by performing side-by-side observations. Today, more than 83 EM27/SUN spectrometers are operated worldwide under COCCON network (Alberti et al., 2022a). The portability of EM27/SUN spectrometer and high accuracy in retrieving XCO<sub>2</sub> and XCH<sub>4</sub> have made the instrument and COCCON network being used in a variety of applications. Pak et al. (2023) and Herkommer et al. (2024) have used EM27/SUN spectrometer as travelling standard to evaluate consistency of TCCON measurements. Frausto-Vicencio et al. (2023) have used EM27/SUN spectrometer to estimate combustion efficiency of wild fires at regional scale. Stremme et al. (2023) have used the spectrometer to study CO<sub>2</sub> plumes from volcano. Dietrich et al. (2021) and Alberti et al. (2022b) have used them for detecting city scale gradient in the gas mixing ratios and identifying the sources of emissions.

An assessment conducted by Buchwitz et al. (2017) using TCCON sites found that GOSAT and OCO-2 meet the requirements set by ESA's CCI Programme and WMO's GCOS implementation plan across various parts of the world. However, due to a lack of data, this systematic assessment has so far not been conducted over South Asia. However, there have been a few studies that compared satellite data with ground-based FTIR observations from Shadnagar (17°05' N, 78°13' E), near Hyderabad, Telangana—a city in the south-central part of India. Sagar et al. (2022) compared XCH<sub>4</sub> values from Sentinel-5P/TROPOMI (from December 2021 to March 2021) with ground-based FTIR observations and found a mean bias of 3.61 ppb. Pathakoti et al. (2024) compared XCO<sub>2</sub> data from the OCO-2 satellite with ground-based FTIR and reported a mean bias of 3.81 ppm and a root mean square error (RMSE) of 6.6 ppm. Pathakoti et al. (2024) used version 8 bias-corrected OCO-2 data. Aside from these few studies, no systematic ground validation of satellite data for GHGs has been conducted over the South Asian region. Additionally, there has been no validation of GOSAT over South Asia.

111 Since the release of version 8 of OCO-2 data, several improvements have been made to the OCO-2 algorithm, and the  
112 latest version (v11.1) is now available to public users ([Jacobs et al., 2024](#)).  
113 National Atmospheric Research Laboratory (NARL), Gadanki and Institute for Meteorology and Climate Research (IMK-  
114 ASF) of Karlsruhe Institute of Technology (KIT), Karlsruhe collaborated to make XCO<sub>2</sub> and XCH<sub>4</sub> measurements over  
115 South India using a portable Fourier Transform Spectrometer (FTS) similar to the one in COCCON network. In this  
116 manuscript, we present a systematic validation of XCO<sub>2</sub> and XCH<sub>4</sub> estimated from GOSAT and OCO-2 over a site in  
117 South Asia using ground-based measurements and using the latest retrieval algorithms.

## 118 2 Instrumentation and Data

119 In this study, a commercial low resolution (0.5 cm<sup>-1</sup>) FTS (Model: EM27/SUN FTS Make Bruker) with modified sun-  
120 tracker and InGaAs detector is used. The spectrometer has high thermal and mechanical stability and 0.5 cm<sup>-1</sup> spectral  
121 resolution in the spectral range 5000 to 9000 cm<sup>-1</sup>. ~~KIT has developed a sun~~ Sun-tracker system developed at KIT uses  
122 that utilizes live sun image to guide sun-tracker of sun on field stop of spectrometer to guide sun-tracker for accurate  
123 position of sun-beam on the field stop of the sun. This allows far more precise sun-tracking even when intensity over the  
124 sun disk is varying due to cloud or other factors. The tracking accuracy achieved is of the order of 11 arc sec (Gisi et al.,  
125 2011). A detailed description of the instrument can be found in Gisi et al. (2012). The instrument used has been calibrated  
126 by performing side-by-side measurements next to the TCCON spectrometer in Karlsruhe. The instrument is calibrated  
127 for specific deviations from nominal instrumental line shape (ILS) and the absence of any other systematic errors is  
128 verified at KIT. Details about the ILS measurement and data analysis as well as the comparison of calibration factors  
129 between the COCCON spectrometers have been discussed in Frey et al. (2019), Sha et al. (2020) and Alberti et al.,  
130 (2022a). Sha et al. (2020) have found a mean bias of -0.18±0.45 ppm and 0.003±0.005 ppm between EM27/SUN and  
131 TCCON instrument for XCO<sub>2</sub> and XCH<sub>4</sub> respectively. The Ratios of XCO<sub>2</sub> and XCH<sub>4</sub> scaling factors derived from side-  
132 by-side measurements between the spectrometer used in this study (Instrument Serial No. 52) and values estimated using  
133 the instrument unit is used in current study (Instrument Sr. No. 52) and the reference the COCCON reference spectrometer  
134 (Instrument Sr. No. 37) IFS 125HR had values of were determined to be 0.999482 and 1.000825, respectively, prior to  
135 the start before the start of the observations at Gadanki (Alberti et al., 2022a0). In addition to solar spectra, measurements  
136 of atmospheric parameters like temperature and pressure were also obtained near the spectrometer.

### 137 2.1 Ground-based FTS

138 The recorded spectra are analysed using retrieval code PROFFAST v2.4 developed at KIT (KIT IMK-ASF 2024a). PROF-  
139 FAST software retrieves the gas amount by fitting solar absorption spectra and scaling the a priori atmospheric profiles  
140 of the gases. It was run using a python interface PROFFASTpylot v1.3 which also takes care of preprocessing of raw  
141 instrument data (Feld et al., 2024; KIT IMK-ASF 2024b). The PROFFAST algorithm is validated in several studies and  
142 used across all the COCCON sites to provide uniform and consistent data processing (Frey et al., 2019; Gisi et al., 2012;  
143 Hase et al., 2004; Sepúlveda et al., 2012; Sha et al., 2020). The spectral windows used for different species are shown in  
144 Table 2 ~~Table 2~~. The algorithm requires vertical profiles of temperature and pressure and a priori estimates of profiles of  
145 species to be estimated. Vertical profiles of temperature and pressure are obtained from National Center for Environmen-  
146 tal Prediction (NCEP) reanalysis data corresponding to the dates of observations. The a priori estimates of species profiles  
147 are obtained from WACCM (Whole Atmosphere Community Climate Model) (Marsh et al., 2013) which is the average  
148 of 40 year monthly mean values for the site. The preprocessing step involves quality check of interferogram, DC correc-  
149 tion, fast fourier transform, phase correction and resampling of the spectra. Each record of raw data is a set of 10 spectra

of which 5 are captured when the mirror is moving forward and 5 are captured when the mirror is moving backward. The interferogram is checked for signal level and source brightness fluctuations also known as DC variability and is removed from further analysis if threshold levels are not met. The other measurement and instrument specific corrections included in the processing are DC correction (correction for the sun brightness fluctuations) (Keppel-Aleks et al., 2007) and the application of instrumental line shape (ILS) parameters (Abrams et al., 1994; Alberti et al., 2022a; Hase et al., 1999; Messerschmidt et al., 2010). As the first step, the columnar concentrations of CO<sub>2</sub>, CH<sub>4</sub>, O<sub>2</sub> and H<sub>2</sub>O in terms of number of molecules per m<sup>2</sup> are retrieved. Then, the CO<sub>2</sub> and CH<sub>4</sub> concentrations are converted to column average mixing ratios by assuming O<sub>2</sub> mixing ratio as 20.95% and normalising CO<sub>2</sub> and CH<sub>4</sub> concentrations with respect to O<sub>2</sub>. This allows for compensating various systematic errors. XCO<sub>2</sub> measurement precision is 0.13 ppmv and XCH<sub>4</sub> measurement precision is 0.6 ppbv (Frey et al., 2019).

Table 2. List of spectral windows used for retrieving columnar concentrations of various gases using ground-based FTS

Species	Spectral windows used for analysis
CH <sub>4</sub>	5897 – 6145 cm <sup>-1</sup>
CO <sub>2</sub>	6173 – 6390 cm <sup>-1</sup>
O <sub>2</sub>	7765 – 8005 cm <sup>-1</sup>
H <sub>2</sub> O	8353.4 – 8463.1 cm <sup>-1</sup>

Observations were carried out from October 2015 to July 2016 in the Gadanki campus of NARL. Gadanki (Latitude: 13.45° N, Longitude: 79.18° E, 360 m above mean sea level) is a rural site in South India with a tropical wet climate. It experiences two monsoon seasons known as southwest and northeast monsoon seasons. Change in wind circulation from one season to the other season is known to have significant effect on trace-gases and aerosol concentrations at the site (Renuka et al., 2014; 2020; Suman et al., 2014). The site is surrounded by hilly terrain and the nearest city is about 35 km away. A major part of the terrain surrounding Gadanki is forest and farm lands. Though there is no farming of rice (paddy field) in the immediate vicinity, the region as a whole has a good number of paddy fields. More details about the site and various atmospheric observation facility can be found in Pandit et al. (2015) and Jayaraman et al. (2010). The FTS observations were carried out from morning to evening at an interval of 1 minute except during days with inclement weather and weekends. More than 39,000 spectra covering a period of 10 months were analysed to retrieve XCO<sub>2</sub> and XCH<sub>4</sub>.

## 2.2 GOSAT

The greenhouse gases observing satellite (GOSAT) also known as IBUKI is a joint project of the Ministry of the Environment (MoE), Japan; the National Institute for Environmental Studies (NIES), Japan and the Japan Aerospace Exploration Agency (JAXA), Japan (Yokota et al., 2009). The main instrument onboard GOSAT is a Thermal and Near infrared Sensor for carbon Observations (TANSO) (Table 1). It is a Fourier transform spectrometer (FTS) with two detectors, one for shortwave infrared (SWIR) wavelength range and the other for thermal infrared (TIR) wavelength range (Olsen et al., 2017). While the TIR sensor is used to retrieve CO<sub>2</sub> and CH<sub>4</sub> profiles, the SWIR sensor is used to retrieve column average dry mole fraction of CO<sub>2</sub> (XCO<sub>2</sub>) and CH<sub>4</sub> (XCH<sub>4</sub>). In the current study, only XCO<sub>2</sub> and XCH<sub>4</sub> values from SWIR sensor are used.

The column-averaged dry-air mole fractions of methane (XCH<sub>4</sub>) and carbon dioxide (XCO<sub>2</sub>) retrieved from GOSAT are available from three different sources: (1) National Institute for Environmental Studies (NIES), Japan, (2) UK National Centre for Earth Observation University of Leicester (UoL), UK, and (3) the Goddard Earth Science Data Information and Services Center (GES DISC) of National Aeronautics and Space Administration (NASA, USA).

**NIES Data Products:**



NIES provides operational XCH<sub>4</sub> and XCO<sub>2</sub> products using a full physics algorithm, which minimizes the difference between observed and simulated spectra generated by a radiative transfer model (Someya et al., 2023). In the current study, we use bias-corrected FTS SWIR Level 2 v3.05 data products from NIES, hereafter referred to as NIES XCH<sub>4</sub> or NIES XCO<sub>2</sub>. The pre-processing involves correction for observation time, pointing anomalies, wave number, sensor degradation, etc., and preparing meteorological data. In the second step, data are screened out for the presence of cloud, high solar zenith angle (> 70°), high ground surface roughness, elevated aerosol layer, etc., along with 13 instrument related quality flags. XCO<sub>2</sub> and XCH<sub>4</sub> values are then retrieved by minimizing difference between observed and simulated spectra.

#### **UoL Data Products:**

UoL provides XCH<sub>4</sub> data derived using a proxy retrieval approach (Parker et al., 2020). This method first retrieves the XCH<sub>4</sub>/XCO<sub>2</sub> ratio from the common absorption band near 1.6 µm, and then estimates XCH<sub>4</sub> by multiplying this ratio with a model-derived XCO<sub>2</sub> value. The advantage of this approach is its reduced sensitivity to aerosols, thin cirrus clouds and certain instrumental effects. However, reliance on model-based XCO<sub>2</sub> can introduce biases in the retrieved XCH<sub>4</sub>. To mitigate this, UoL uses the median of XCO<sub>2</sub> estimates from three different atmospheric models constrained by surface in-situ observations. In the current study, we use UoL Version 9 XCH<sub>4</sub> data, hereafter referred to as UoL XCH<sub>4</sub>.

#### **NASA ACOS Data Products:**

NASA's GES DISC The Goddard Earth Science Data Information and Services Center of National Aeronautics and Space Administration (NASA, USA), USA provides XCO<sub>2</sub> products data-retrieved from GOSAT satellite's SWIR sensor under the Atmospheric CO<sub>2</sub> Observations from Space (ACOS) project (Osterman et al., 2017), using a full physics algorithm originally developed for the OCO satellite and later adapted for GOSAT. In the current study, we use In this study, FTS SWIR L2 v3.05 XCO<sub>2</sub> and XCH<sub>4</sub> bias corrected data products from National Institute for Environmental Studies (NIES), Japan and ACOS Level 2 bias-corrected XCO<sub>2</sub> version Version v9.2 data full physics retrieval data from Goddard Earth Sciences Data and Information Services Center are used, hereafter referred to as ACOS XCO<sub>2</sub>.

### **2.3 OCO-2**

Orbiting Carbon Observatory-2 (OCO-2) is NASA's Earth remote sensing satellite to study atmospheric carbon dioxide from space (Crisp et al., 2004). In the current work, we have used processed and bias corrected data version 11.1r downloaded from the website of ~~Goddard Earth Science Data Information and Services Center (GES DISC;~~ (<http://disc.gsfc.nasa.gov/>). Version 11.1r is the latest version of data which were released in May 2023. The version 11.1r data contains retrospectively retrieved XCO<sub>2</sub> values using full physics algorithm with several improvements with respect to its predecessor algorithms (Jacobs et al., 2024; Payne et al., 2023). The OCO-2 was launched on July 2, 2014 in sun-synchronous orbit with equatorial crossing time at 13:30 on an ascending node with 16 days repeat cycle (Table 1). OCO-2 instrument consists of three boresight high resolution imaging grating spectrometers which provides high resolution spectra of reflected sun light in oxygen A band (0.765 µm) and in two CO<sub>2</sub> bands at 1.61 and 2.06 µm. The instruments can be operated in three modes viz., target, glint and nadir. The ground resolution varies depending on the mode of operation. In the current study, data from the nadir mode are used which has the spatial resolution of 1.29 km x 2.25 km (Crisp et al., 2017). The spectra are corrected for various artefacts such as bad pixels, cosmic ray artefacts and converted to radiometric values. Using full physics radiative transfer model, synthetic spectra are produced and compared with observed spectra. An inverse model iteratively modifies the assumed atmospheric state to improve the fit. The number densities of CO<sub>2</sub> and O<sub>2</sub> thus retrieved are used to get XCO<sub>2</sub> by taking ratio of them and multiplying it by 0.2095. The retrieval is further applied bias correction obtained from collocated TCCON data, models and small area analysis (O'Dell et al., 2018). More details of the retrieval process are available in Crisp et al. (2021). The OCO-2 data are distributed in

two formats known as standard files and Lite files. The standard files contain CO<sub>2</sub> mixing-ratios without bias correction whereas mixing-ratios in the Lite files are bias corrected (Payne et al., 2023). The data files contain a quality flag for each retrieval. The quality flag value “0” corresponds to good data, whereas the quality flag value “1” suggests the presence of any of the 24 algorithmically identified quality issues in the retrieved value. In the present work, we have used bias corrected data with quality flag “0” only.

### 3 FLEXPART (A Lagrangian Particle Dispersion Model)

Besides, comparing satellite data with ground-based observations, we have also examined the seasonal variation of methane mixing ratios using a Lagrangian Particle Dispersion Model to understand the influence of local sources vis-a-vis long-range transport. The FLEXPART (Pisso et al., 2019), an open source model developed at [Norwegian Institute for Air Research \(NILU\), Kjeller, Norway](#) is widely used by the research community around the world to identify the source regions of long range transport. The model takes meteorological fields as input and tracks the movement of virtual particle forward or backward in time. The particle can be configured to represent a gas or aerosols of one’s choice and accordingly be subjected to various physical processes such as advection, turbulence, dry deposition, wet deposition, radioactive decay, etc. Except for reaction with OH radical no other chemical transformation is modelled in FLEXPART.

We configured FLEXPART for backward-in-time run from observation site (Gadanki) with virtual particle representing methane molecules. The backward-in-time runs provide a source-receptor relationship which can be used to calculate mixing ratios or concentrations at observation site using emission fluxes. The model run is configured such that mixing ratios thus calculated represent results of emissions within the past 10 days and average of 0 to 15 km atmospheric column at the observation site. This configuration effectively captures most regional emissions and tropospheric methane mixing ratios. Using few sensitivity tests, we have found that emissions within 10 to 15 days have insignificant contribution to concentrations beyond 15 km. More details of the model settings used for the current study are provided in [Table 3](#).

**Table 3. The FLEXPART model setup and the input data details**

Input Meteorological Data	ECMWF Reanalysis – Interim (ERA-Interim) (Dee et al., 2011)
Tracer	CH <sub>4</sub>
Point of origins for retroplume (aka Release Point)	Gadanki Latitude: 13.45° N Longitude: 79.18° E, Site altitude: 365 m a. s. l. Plume release altitudes from ground: 0 – 15 km.
Number of particles released for each day	100000
Mode	Backward runs
Number of days backward for each release	10 days
User selectable Processes	Dry Deposition – disabled Convection – enabled Wet deposition – disabled Reaction with OH radical – enabled
OH reaction related settings	Constants $C = 9.65 \times 10^{-20} \text{ cm}^3 \text{ molecule}^{-1} \text{ sec}^{-1}$

D = 1082.0 K N = 2.58 (no unit)
------------------------------------

### 3.1 ECLIPSEv6 inventory

In order to calculate the concentrations resulting from recent regional emissions (emissions within past 10 days of a given observation), we used ECLIPSEv6b (Evaluating the CLimate and air quality ImPacts of Short-livEd pollutants version 6b) emission inventory (Amann et al., 2011, 2012; Klimont et al., 2017; Hoglund-Isaksson, 2012; Stohl et al., 2015). The inventory is prepared following IPCC (2008) recommended method and using [Greenhouse Gas - Air Pollution Interactions and Synergies \(GAINS\)](#) model (Amann et al., 2011). [It provides sector-specific anthropogenic emission estimates for 11 species, including CH<sub>4</sub>, across eight economic sectors.](#) The data are provided as 0.5° x 0.5° gridded values for the years from 1990 to 2050 at an interval of 5 years for two scenarios namely current legislation for air pollution, which is also the reference scenario and maximum technically feasible reductions scenario. The latest version ([Version 6b](#)) was released in August 2019 and incorporates updates for historical data, new waste sectors, soil NO<sub>x</sub> emissions, international shipping emissions and energy-macroeconomic data. The inventory includes only anthropogenic emission fluxes from sectors viz. energy, industry, solvent use, transport, domestic combustion, agriculture, open biomass and agricultural waste burning, and waste treatment. Natural emissions from wetlands, forest fires, biogenic emissions, etc. are not included in the inventory. The total Global, South Asia (members of SAARC – South Asian Association for Regional Cooperation), and India's emissions of methane for the year 2015 were 336.2, 44.2 and 31.5 Tg, respectively.

### 3.2 Wetland Inventory

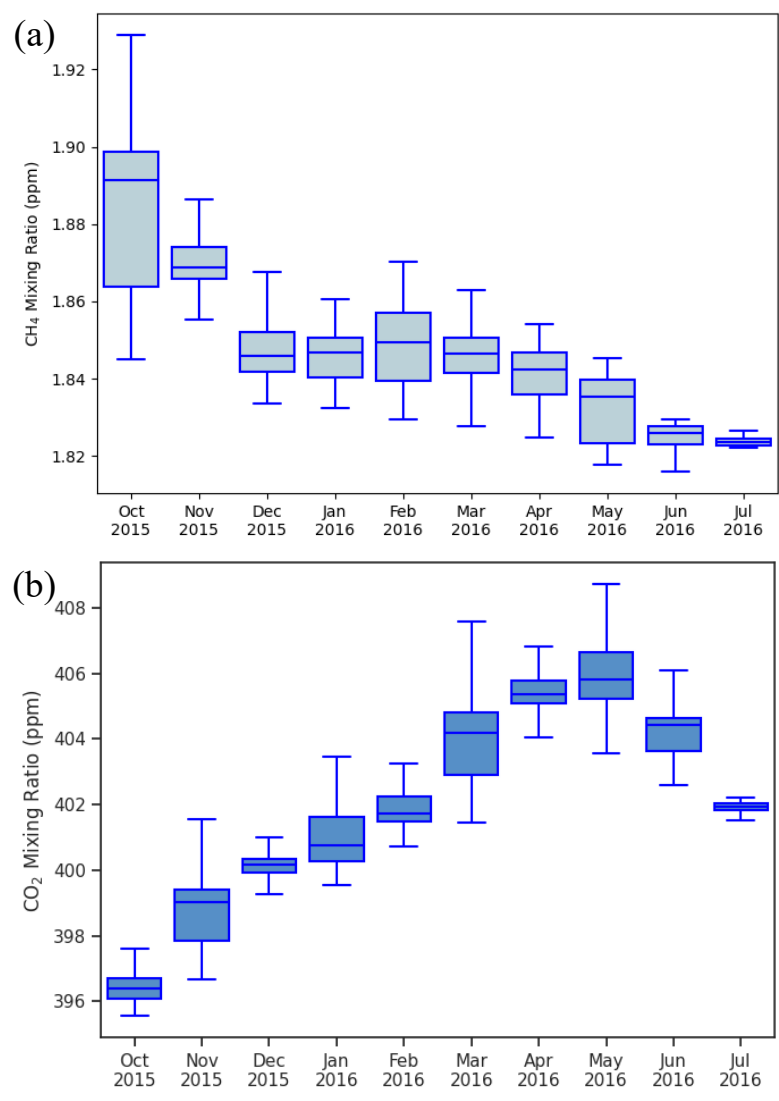
The emissions from wetlands can contribute significant atmospheric load of methane at the observation site and hence in addition to anthropogenic emissions from ECLIPSEv6 inventory, we used [Wetland CH<sub>4</sub> emissions and uncertainty dataset for atmospheric chemical transport models \(-WetCHARTs\)](#) version 1.0 inventory (Bloom et al., 2017a, b) for calculating methane concentrations at Gadanki from recent emissions. The inventory contains global monthly emission fluxes of methane at 0.5° by 0.5° resolution for ensemble of multiple terrestrial biosphere models, wetland extent scenarios and temperature dependencies. The emission fluxes from 2001-2015 are provided for three choices of global scaling, two choices of wetland spatial extent, two choices for temporal variability of wetland extent, nine choices of heterotrophic respiration schemes and three choices of parametrization scheme for temperature dependency. In the current work, we have used data corresponding to the scaling factor with global emissions 166 TgCH<sub>4</sub> yr<sup>-1</sup>, CARDAMOM (CARbon DAta MOdel fraMework) terrestrial C cycle analysis for heterotrophic respiration (Bloom et al., 2016), mid-range temperature sensitivity and, spatial and temporal extent of wetlands constrained with SWAMPS (Surface WATER Microwave Product Series) multi-satellite surface water product (Schroeder et al., 2015). These choices are made based on following consideration. Choice of scaling factor represents the mid-point global emissions among the three choices available viz. 124.5, 166 and 207.5 Tg CH<sub>4</sub>/yr. While there are nine choices for heterotrophic respiration, there is only one choice available for emission fluxes after 2010 which is CARDAMOM and used here. Between the two choices of spatial extent and two choices of temporal variability, the SWAMPS multi-satellite surface water product is used because it represents observationally constrained inundated areas including lakes and other water bodies.

## 4 Results and Discussion

Box plots of monthly statistics are shown in [Figure 1](#) for (a) XCH<sub>4</sub> and (b) XCO<sub>2</sub> measured by EM27/SUN at the Gadanki site. [Figure 2](#) shows the time series of hourly mean values of XCH<sub>4</sub> and XCO<sub>2</sub> from EM27/SUN, [NIES](#),



285 UoL, ACOS and OCO-2, ~~ACOS and GOSAT~~ within box size  $\pm 30^\circ$  longitude and  $\pm 10^\circ$  latitude of the site (Table 4). A  
 286 large variability in  $XCH_4$  values is observed in October, but in other months, the variability is relatively low. The median  
 287 values of  $XCH_4$  are found to systematically decrease from 1.892 ppm in October to 1.826 ppm in June of the following  
 288 year, with similar values observed in July. The monthly median values of  $XCO_2$  increased from 396.4 ppm in October to  
 289 405.8 ppm in May, then began to decrease after May. Unlike  $XCH_4$ , the  $XCO_2$  values did not show high variability in  
 290 October. A similar seasonal variation was observed by Jain et al., (2021) in surface mixing ratios of  $CO_2$  and  $CH_4$  at  
 291 Gadanki. Kavitha and Nair (2016) using SCIAMACHY satellite data over India for the period 2003-2009, also reported  
 292 similar seasonal variations, attributing them to regional rice cultivation patterns. Further discussion on the seasonal vari-  
 293 ation is provided in the subsequent section.



294  
 295 **Figure 1. Box plot of monthly statistics of (a)  $CH_4$  and (b)  $CO_2$  columnar mixing ratios observed at Gadanki, India using**  
 296 **ground-based FTIR.**

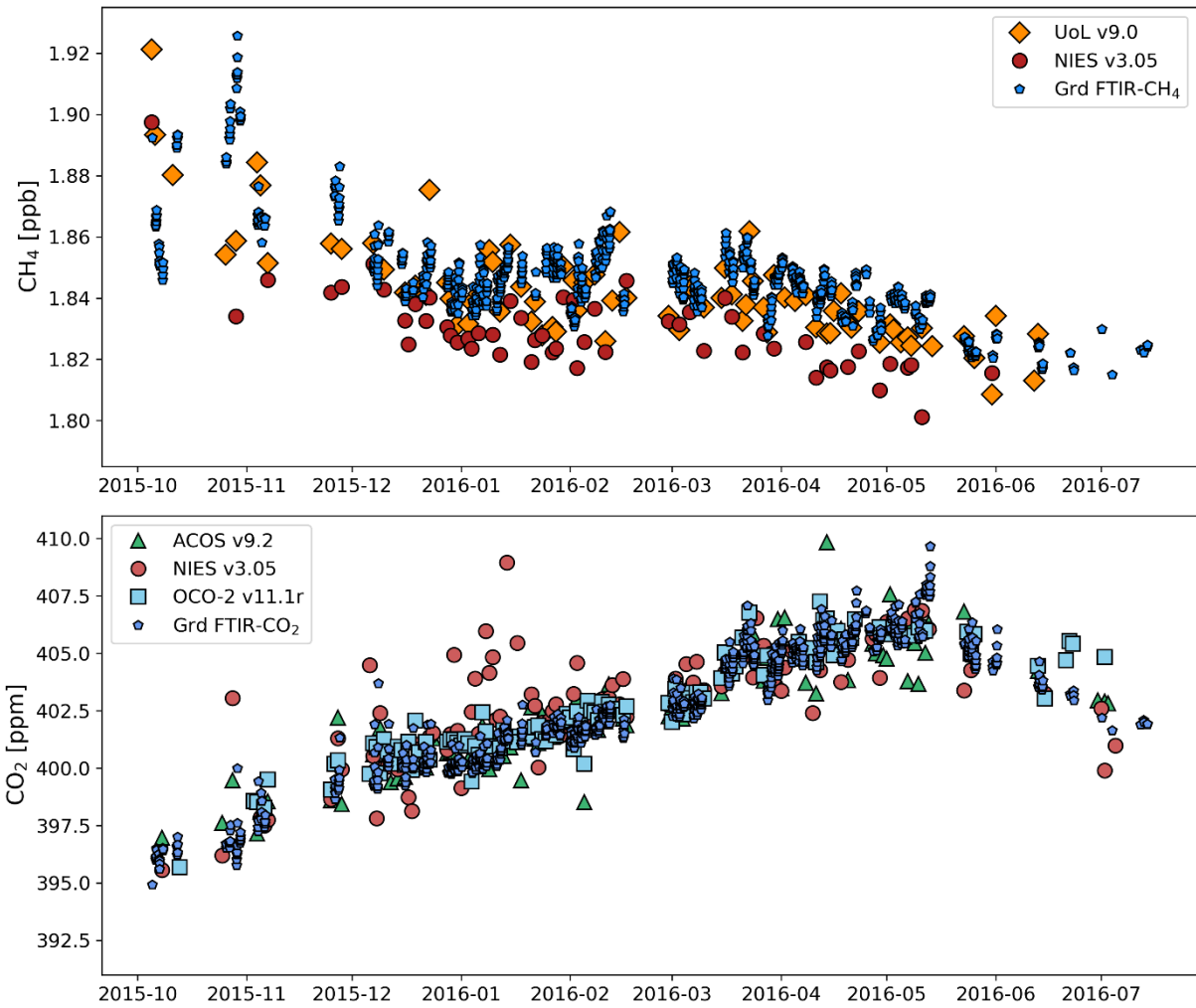


**Figure 2. Hourly mean values of columnar CH<sub>4</sub> (top) and CO<sub>2</sub> (bottom) mixing ratios observed using ground based FTIR along with paired satellite observations. See the text for description of pairing method (~~GOSAT data version 3.05; OCO-2 data version v11.1r; ACOS v9.2~~; Box size  $\pm 30^\circ$  longitude and  $\pm 10^\circ$  latitude)**

#### 4.1 Comparison of satellite-based and ground-based mixing-ratios

The GOSAT satellite ~~revisits~~ observes the same point on Earth every three days, ~~with and gas retrievals are performed~~ only under ~~clear cloud-free~~ sky conditions. This limits the number of concurrent ~~satellite and observations available with~~ ground-based FTIR ~~measurements~~. To ~~overcome address~~ this limitation and ensure sufficient ~~number of paired data pairs~~ ground-and-satellite data for comparison, we have followed an approach similar to Buchwitz et al. (2017). This approach relies on the fact that CO<sub>2</sub> and CH<sub>4</sub> have long atmospheric residence times, allowing the history of air parcels to be used to pair data for comparison.

In this approach, the first step is to identify all satellite data within a certain distance of the ground station. Buchwitz et al. (2017) used satellite data within  $\pm 30^\circ$  longitude and  $\pm 10^\circ$  latitude of TCCON sites to evaluate GOSAT and OCO-2 data products. Wunch et al. (2017) used box of  $\pm 5^\circ$  longitude and  $\pm 2.5^\circ$  latitude around the TCCON sites in the Northern Hemisphere and  $\pm 60^\circ$  longitude and  $\pm 10^\circ$  latitude around the TCCON sites in the Southern Hemisphere to evaluate XCO<sub>2</sub> estimates from the OCO-2 satellite. In the second step, ground-based observations taken within three days of the satellite overpass and during same time of the day (within two hours) ~~of the same time of day~~ are paired with the satellite data. In the third step, the data pairs obtained in step 2 are further filtered using the criterion that the CAMS model output of XCH<sub>4</sub> and XCO<sub>2</sub> values, interpolated to the satellite location and ground station, cannot differ by more than 0.25 ppm for XCO<sub>2</sub> and 5 ppb for XCH<sub>4</sub>, respectively. This third step is based on the premise that the CAMS model is capable of simulating transport accurately, meaning that while the absolute values may not always be correct, the spatial variability

in the model is reliable. The criteria in step 3 ensures that satellite and ground values are only compared when they share the same air mass history. It should be noted that the absolute value of the model simulation and its differences with observations are not relevant in this step. More detailed discussions on the need and the rationale behind this complex approach for data pairing can be found in Nguyen et al. (2014) and Wunch et al. (2011b). A sensitivity test, described in Table S1 of the Supplement, shows omitting the model-based air mass filtering (Step 3) increases the number of matched pairs by factors of 2 – 3 across species and datasets. While the effect on bias is mixed, the scatter generally increases slightly when Step 3 is not applied. For consistency with previous studies, we report results based on the full three-step pairing procedure.

We note that no averaging kernel (AK) correction were applied in this analysis. While applying AK corrections is ideal to account for vertical sensitivity differences between satellite and ground-based retrievals, effect of their omission is expected to be small for our study location. Sha et al. (2021) demonstrated that at low-latitude sites, the impact of smoothing and a priori profile differences on XCH<sub>4</sub> biases is minor, typically below -0.25%, with an average effect of -0.14%. Given that Gadanki (13.5° N) is a low-latitude station, the lack of AK correction is unlikely to significantly affect our conclusions.

We performed calculations for three different box sizes around the observation site at Gadanki (13.45° N, 79.18° E): ( $\pm 5^\circ$  longitude,  $\pm 2.5^\circ$  latitude), ( $\pm 10^\circ$  longitude,  $\pm 5^\circ$  latitude), and ( $\pm 30^\circ$  longitude,  $\pm 10^\circ$  latitude). By the end of the third step, we obtained 55 pairs of XCH<sub>4</sub> from GOSAT NIES v3.05, 81 pairs of XCH<sub>4</sub> from GOSAT UoL v9, 117 pairs of XCO<sub>2</sub> from GOSAT v3.05, 1178 pairs of XCO<sub>2</sub> from ACOS v9.2 and 120 pairs of XCO<sub>2</sub> from OCO-2 v11.1 for the biggest box-size in Step 1 (see Table 4, Figure 2). The number of data pairs for XCO<sub>2</sub> is more than double that of XCH<sub>4</sub> for all box-sizes. This difference reflects the fact that carbon dioxide has a much longer atmospheric lifetime (>100 years) compared to methane (~12 years).

**Table 4: Mean bias and scatter between satellite and ground-based measurements. Values that meet CCI criteria are shown in bold letters.**

Satellite	Species	Product version	Box Size for pairing		Number of data points	Bias = mean (Xsat - Xgrd)*	Scatter = stddev(Xsat - Xgrd)*	Pearson correlation coefficient R
			Longitude	Latitude				
GOSAT	XCH <sub>4</sub>	<u>NIES v3.05</u>	$\pm 30$	$\pm 10$	55	-18.5 ppb	<b>13.8 ppb</b>	0.47
			$\pm 10$	$\pm 5$	19	<b>-9.07 ppb</b>	<b>12.1 ppb</b>	0.75
			$\pm 5$	$\pm 2.5$	12	-12.8 ppb	<b>6.21 ppb</b>	0.85
		<u>UoL v9.0</u>	<u><math>\pm 30</math></u>	<u><math>\pm 10</math></u>	<u>81</u>	<u><b>-5.6 ppb</b></u>	<u><b>15.0 ppb</b></u>	<u>0.58</u>
			<u><math>\pm 10</math></u>	<u><math>\pm 5</math></u>	<u>39</u>	<u><b>-0.6 ppb</b></u>	<u><b>13.6 ppb</b></u>	<u>0.7</u>
			<u><math>\pm 5</math></u>	<u><math>\pm 2.5</math></u>	<u>24</u>	<u><b>-2.0 ppb</b></u>	<u><b>7.9 ppb</b></u>	<u>0.86</u>
	XCO <sub>2</sub>	<u>NIES v3.05</u>	$\pm 30$	$\pm 10$	117	0.644 ppm	<b>1.69 ppm</b>	0.74
			$\pm 10$	$\pm 5$	59	0.812 ppm	<b>1.88 ppm</b>	0.59
			$\pm 5$	$\pm 2.5$	27	0.983 ppm	<b>1.59 ppm</b>	0.67
		ACOS v9.2	$\pm 30$	$\pm 10$	1178	<del>0.163</del> <u><b>0.156 ppm</b></u>	<b>1.09 ppm</b>	0.90
			$\pm 10$	$\pm 5$	54	<b>0.077 ppm</b>	<b>1.25 ppm</b>	0.86
			$\pm 5$	$\pm 2.5$	<del>2438</del>	<b>-0.212 ppm</b>	<b>1.02 ppm</b>	0.90
		V11.1r	$\pm 30$	$\pm 10$	120	<b>0.408 ppm</b>	<b>0.776 ppm</b>	0.94

OCO-2	XCO <sub>2</sub>		±10	±5	67	<b>0.342 ppm</b>	<b>0.806 ppm</b>	0.94
			±5	±2.5	41	<b>0.163 ppm</b>	<b>0.786 ppm</b>	0.95
*Xsat are satellite based mixing ratio estimates and Xgrd are ground based FTIR mixing ratio estimates. For all the satellites, their bias corrected values are used.								

With the paired dataset in place, we ~~now assess~~ evaluated the bias, scatter, and correlation between satellite and ground-based measurements, as summarized in Table 4. Here, The bias is defined as the mean of difference between ~~the~~ satellite- and the ground-based dry-air mole fractions, mixing-ratio, the scatter ~~as is defined as~~ the standard deviation of these differences, and ~~the correlation as~~ coefficient between ground and satellite data is the Pearson correlation coefficient (R) between the paired values. The European Space Agency's ~~The Climate Change Initiative (ESA CCI) of ESA has specified~~ performance targets of precision (scatter) and systematic error (bias) requirements of < 34 ppb for scatter (precision) and < 10 ppb for bias (systematic error) for XCH<sub>4</sub>, and <8 ppm for scatter and <0.5 ppm for bias for XCO<sub>2</sub> (Chevallier et al., 2016). ~~Statistically significant correlation exists between ground-based and satellite measurements for all box sizes (Table 4).~~

#### XCH<sub>4</sub> Validation Results

For GOSAT NIES XCH<sub>4</sub>, biases ranged from -9 ppb to -18.5 ppb depending on the spatial window size. For GOSAT UoL XCH<sub>4</sub>, biases were notably lower, ranging from -0.6 ppb to -5.6 ppb. While larger spatial windows provided more matched pairs, they did not consistently yield lower bias or scatter. In fact, the intermediate box size (±10° x ±5°) showed the lowest bias and scatter for both products. Importantly, biases across all box sizes remained within one standard deviation of the smallest box size, indicating that larger spatial windows may not offer significant additional value, particularly when longer time series of ground-based data are available.

The UoL XCH<sub>4</sub> product met the ESA CCI bias requirement (< 10 ppb) across all box sizes. In contrast, the NIES XCH<sub>4</sub> products met this requirement only for the intermediate box, with marginal exceedances for the smallest box. Scatter values ranged from 6 ppb to 15 ppb across products and box sizes, well within the CCI precision requirement of 34 ppb.

Although derived from the same satellite, the

~~The bias in GOSATv3.05 XCH<sub>4</sub> data is -9.07 ppb for the 20° x 10° longitude-latitude box size, meeting the CCI requirement, though it was larger for the other box sizes. The scatter requirement of < 34 ppb is met with a significant margin for all box sizes. The scatter ranged from 6.2 ppb to 13.8 ppb from the smallest to the largest box size. UoL XCH<sub>4</sub> product, which uses a proxy retrieval approach, showed substantially improved bias performance compared to the NIES product. However, its scatter was slightly higher (approx. 2 ppb) than the NIES product for equivalent spatial windows ranging from 8 to 15 ppb.~~

#### XCO<sub>2</sub> Validation Results

All XCO<sub>2</sub> products showed high correlation with ground-based measurements across all spatial windows. Biases for The ~~correlation between~~ GOSAT NIES XCO<sub>2</sub> ranged from 0.644 ppm to 0.983 ppm, exceeding the CCI bias threshold of 0.5 ppm for all box sizes. However, scatter values (1.59–1.88 ppm) were well below the 8 ppm precision requirement.

~~and ground-based XCO<sub>2</sub> is significant for all the box sizes used for data pairing. The Climate Change Initiative (CCI) of ESA has specified precision (scatter) and systematic error (bias) requirements of < 8 ppm and < 0.5 ppm for XCO<sub>2</sub> (Chevallier et al., 2016). The bias is lowest, at 0.644 ppm, for the largest box size (60° long x 20° lat) and highest, at 0.983 ppm, for the smallest box size (10° long x 5° lat). The larger box sizes correspond to the criteria set by Buchwitz et al. (2017), while the smaller box sizes correspond to Wunch et al. (2017). Neither meets the CCI listed systematic error (bias) requirements of < 0.5 ppm. However, the scatter requirement of < 8 ppm is comfortably met. The scatter values for GOSATv3.05 XCO<sub>2</sub> are in the range of 1.59 ppm to 1.88 ppm.~~

379 In contrast, ACOS version 9.2 XCO<sub>2</sub> values, also based on which are derived from the GOSAT observations but using  
 380 satellite but use a different retrieval algorithm, demonstrated superior performance. significantly better than the GO-  
 381 SAT v3.05 values. Biases values ranged from -0.212 ppm to 0.163 ppm, meeting the CCI bias requirement across all box  
 382 sizes, and scatter values ranged from 1.02 ppm to 1.25 ppm, also comfortably within the precision target. depending on  
 383 the longitude-latitude box size. The correlation coefficient (R = 0.86–0.90) for ACOS XCO<sub>2</sub> were higher than those for  
 384 NIES XCO<sub>2</sub> (R = 0.59 – 0.74) values is also far superior. The correlation coefficient values for ACOS v9.2 XCO<sub>2</sub> are  
 385 between 0.86 and 0.9, whereas the correlation coefficient values for GOSAT v3.05 XCO<sub>2</sub> range from 0.59 to 0.74.  
 386 The correlation of ground data with OCO-2 XCO<sub>2</sub> v11.1r product showed is the highest correlation among all datasets (R  
 387 = 0.94 – 0.95), with biases ranging from 0.163 ppm to 0.408 ppm, fully meeting the CCI bias target. Scatter values (0.776  
 388 – 0.806 ppm) were the lowest among all products evaluated. among the three satellite XCO<sub>2</sub> datasets evaluated. The cor-  
 389 relation coefficients (R values) for OCO-2 XCO<sub>2</sub> v11.1r are between 0.94 and 0.95. The biases also meet the CCI require-  
 390 ment of < 0.5 ppm, though they are slightly larger than those for ACOS XCO<sub>2</sub>. The biases for OCO-2 XCO<sub>2</sub> range from  
 391 0.163 ppm to 0.408 ppm for different longitude-latitude boxes.  
 392 Our results for OCO-2 XCO<sub>2</sub> differ notably from the higher bias of 3.81 ppm reported by Pathakoti et al. (2024) for  
 393 Shadnagar, India, located about 500 km north of our study site. While Pathakoti et al. have not discussed the reason for  
 394 such a high bias in their study, it is unlikely to be solely due to the use of an earlier version of the OCO-2 dataset by them.  
 395 Pairing methodology differences between our study and that of Pathakoti et al. may have contributed to the difference in  
 396 results. Their study used a smaller spatial window (4° × 4°) and daily mean ground-based values, whereas we applied a  
 397 larger spatial window (10° × 5°), used hourly collocation within ±2 hours, and applied model-based air mass filtering to  
 398 improve representativeness. Additionally, Pathakoti et al. did not specify the retrieval algorithm version for their ground-  
 399 based FTS data. Pak et al. (2023) have shown that using GGG2020 instead of GGG2014 reduces XCO<sub>2</sub> bias from 1.3  
 400 ppm to 0.5 ppm, which may further explain the discrepancy.  
 401  
 402 The scatter for OCO-2 ranges from 0.776 ppm to 0.806 ppm, depending on box size, and is significantly smaller than  
 403 both the GOSAT XCO<sub>2</sub> v3.05 and ACOS XCO<sub>2</sub> v9.2 values, meeting the CCI criteria of < 8 ppm.  
 404 Figure 3 Figure 3 shows the time series of biases for XCH<sub>4</sub> and XCO<sub>2</sub> biases for using a the ±30° × ±10° longitude-latitude  
 405 box around Gadanki. No systematic changes in biases are observed for most products, both XCH<sub>4</sub> and XCO<sub>2</sub> except for.  
 406 GOSAT NIES XCO<sub>2</sub>, values which exhibited positive biases during December to February and negative biases during  
 407 April to May. Overall, the biases at the Gadanki location are consistent with those (–1 ppm) reported by O' Dell et al.  
 408 (2018) for OCO-2 version 8 data over TCCON sites (~ 1 ppm).



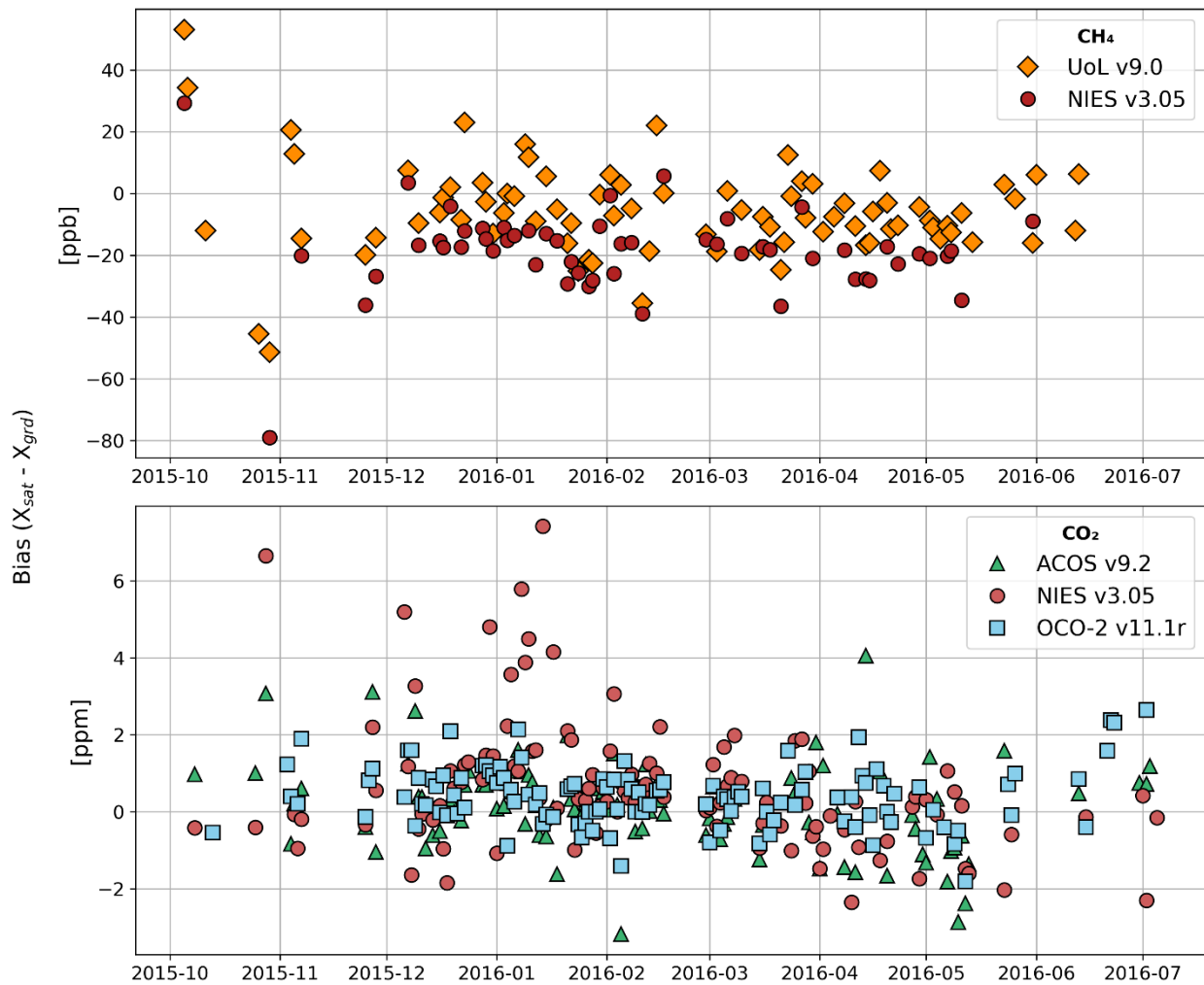


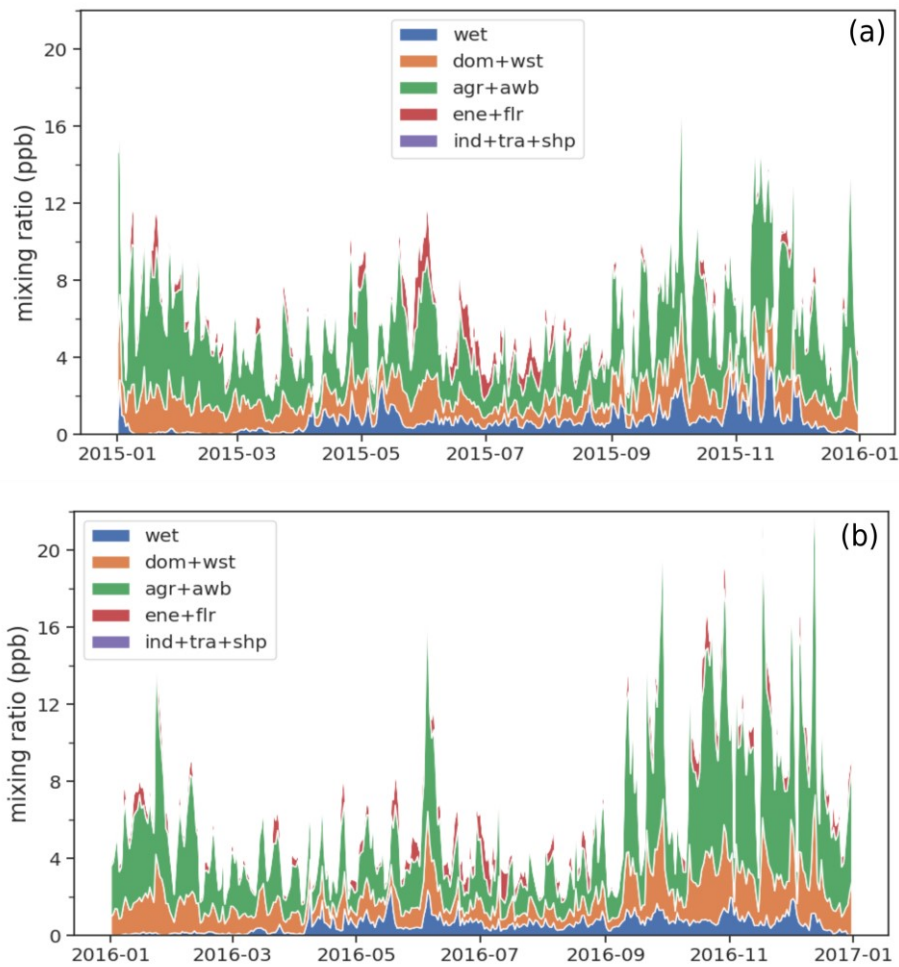
Figure 3: Time series of biases in GOSAT and OCO-2 retrieved  $X_{CH_4}$  (top panel) and  $X_{CO_2}$  (bottom panel) values over Gadanki, India. Values-Results are shown for satellite data selected within a  $\pm 30^\circ$  longitude and  $\pm 10^\circ$  latitude region centred on around the station.

#### 4.2 Case Studies and Seasonal variations of methane

Figure 4 shows methane mixing ratio enhancements calculated using the FLEXPART model and the ECLIPSEv6+Wetland inventory. As previously mentioned, the model is configured such that the values represent daytime mean mixing-ratios in the altitude range of 0 to 15 km over Gadanki, contributed by emissions from the preceding 10 days. The altitude range of 0 to 15 km is selected because the tropopause altitude in the tropics is typically between 15 and 18 km (Pandit et al., 2014), and emissions from the past 10 days are generally confined within this range.

The 10-day back trajectory is chosen based on earlier work by Gadhavi et al. (2015), which demonstrated that, for the Gadanki location, a 10-day back trajectory captures emissions from almost the entire South Asia. The averaging period is selected as daytime (9 am to 6 pm local time) to ensure a one-to-one correspondence with observed mixing ratios, which are measured using solar radiation through FTS and are therefore only available during daylight hours.

Hereafter, these values will be referred to as model values. However, it is important to note that the model values do not account for the columnar  $CH_4$  mixing ratio resulting from emissions prior to the 10-day period and, therefore, do not represent the total columnar mixing ratio as seen in FTS or satellite data.



425

426 **Figure 4: Model calculated columnar (0 to 15km) average methane mixing ratio enhancements due to emissions of past 10 days**  
 427 **for year (a) 2015 and (b) 2016. Colours show contribution of different sectors viz. wetland (wet), domestic+waste (dom+wst),**  
 428 **agriculture + agricultural waste burning (agr+awb), energy + flaring (ene+flr), and industry + transport + shipping**  
 429 **(ind+tra+shp).**

430 Overall, the model estimates methane mixing ratio enhancements ranging from 2 ppb to 26 ppb during 2015 and 2016.  
 431 While there is significant day-to-day variability, a seasonal pattern is still discernible in the model-calculated values.  
 432 Typically, the mixing ratio enhancements are high in November, decreases slightly in December, and rise again during  
 433 January and February. They decrease in March and April, briefly rise in the second half of May, and then decrease again,  
 434 remaining low from June to September. The mixing ratios rise again in October, peaking in November. Sector-wise,  
 435 wetlands do not show large seasonal variations. Wetland contributions are low from December to March. In other seasons,  
 436 wetland contributions occasionally reach as high as 40% of total mixing ratios, but for most part of the year, they remain  
 437 around 10%. The highest contribution comes from the agriculture sector, accounting for nearly 55% of the total mixing  
 438 ratio enhancements, followed by the waste sector, which contributes about 17% to the model values at Gadanki. The  
 439 domestic and energy sectors contribute about 5% each. The domestic sector's contribution is lower in July and August,  
 440 mainly due to the air masses originating from the west of Gadanki in peninsular India, where the population is smaller  
 441 and contributes less to methane emissions. Flaring contributes negligibly for most part of the year, but during June to  
 442 July, its contribution can reach up to 40%, primarily due to low emissions from other sectors during this period and the  
 443 winds from the Arabian Sea bringing emissions from oil rigs off the west coast of India, the eastern Arabian Peninsula,  
 444 and northeastern Africa. Industry, transport, shipping and agricultural waste burning activities contribute less than 1% of  
 445 atmospheric load of methane at Gadanki.

446 **Figure 5** ~~Figure 5~~ shows model-calculated methane mixing ratio ( $\Delta\text{XCH}_4$ ; solid blue line; left Y-axis) and the methane  
 447 mixing ratios ( $\text{XCH}_4$ ) observed using FTS (red filled circles; right Y-axis) in a single plot. The left Y-axis represents the  
 448 model mixing ratio, which only accounts for emissions from the preceding 10 days. For lack of a better term, we refer to  
 449 it as  $\Delta\text{XCH}_4$ . The right Y-axis shows the observed values in ppm. As mentioned earlier, the model was configured to  
 450 reflect incremental variability caused by regional emissions. If the background  $\text{CH}_4$  mixing ratios were constant, the day-  
 451 to-day variability relative to background values should be the same in both the model and the observations. However, we  
 452 observe differences in both the absolute values of variability and their seasonal patterns. Several sudden increases in the  
 453 model values, which appear as spikes in **Figure 5** ~~Figure 5~~ (e.g. 5 October 2015 and 27 December 2015), correspond to  
 454 ~~increase or decrease~~ variations in the observations. While the observations are not as continuous as model values and  
 455 cannot capture all the variability seen in the model, some degree of day-to-day variability is correlated between the model  
 456 and observations ( $R^2 = 0.35$ ). However, the magnitude of variability between the model and observed values is quite  
 457 different. For instance, the observed mixing ratios from 5 October 2015 to 8 October 2015 decreased by 49 ppb, whereas  
 458 the model values during the same period decreased only by 16 ppb. Over the entire observation period, ~~observed-total~~  
 459 column methane mixing ratios ~~values~~ varied by 100 ppb, while the model values which excludes background mixing  
 460 ratios varied only by 20 ppb. This discrepancy may be due to two main factors: either the emission fluxes in the emission  
 461 inventory are underestimated, or the background mixing ratios are not constant. The latter factor could explain the mis-  
 462 match on a monthly scale. Starting in October 2015, both model and observed values are high and decrease toward June-  
 463 July 2016. While the model values are already low by March 2016, the observed values decrease gradually from Novem-  
 464 ber 2015 to January 2016, remain nearly constant from January 2016 to April 2016, and then decrease rapidly in May,  
 465 reaching a minimum during the last week of June and the first week of July.

466 Chandra et al. (2017) analysed methane variations over different parts of India using Japan Agency for Marine-earth  
 467 Science and TEChnology (-JAMSTEC)'s- Atmospheric Chemical Transport Model. They found that, over South India,  
 468 although 60% of the columnar concentration is attributed to  $\text{CH}_4$  in the lower troposphere, there is very little correlation  
 469 between regional emissions and columnar methane variations. This was attributed to changes in atmospheric chemistry  
 470 and transport. According to Chandra et al. (2017), the methane loss rate increases from 6 ppb day<sup>-1</sup> in January to 12 ppb  
 471 day<sup>-1</sup> from April to September. Additionally, anticyclonic winds in the upper troposphere confine uplifted methane mol-  
 472 ecules over broader South Asia during the monsoon season, contributing significantly to methane over Western India, but  
 473 not significantly over South India. Since ~~the~~ FLEXPART doesn't include chemistry other than the reaction with OH  
 474 radical, lower decrease in model values from March to July could be due to absence of chemistry as well as transport of  
 475 background methane above 15 km.

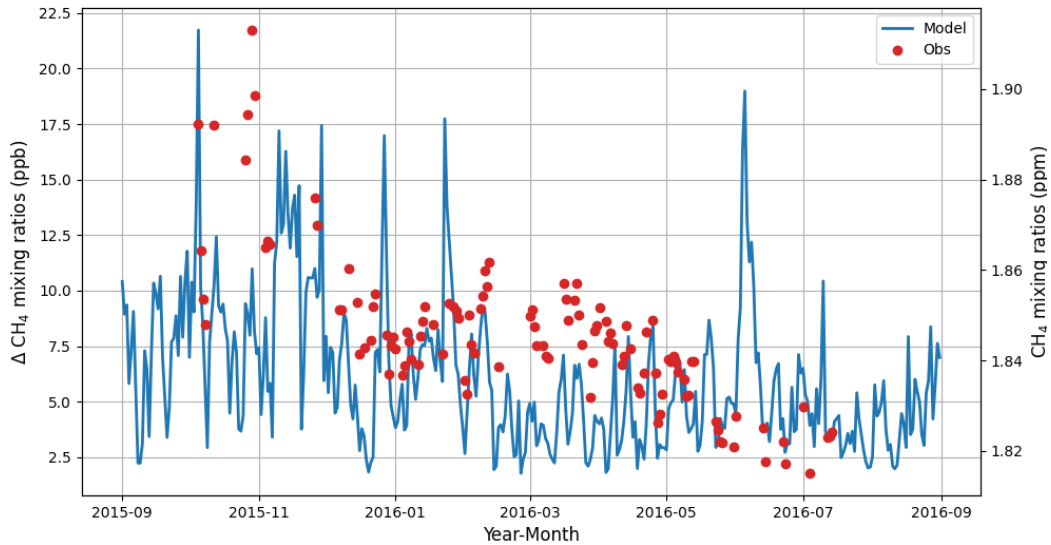


**Figure 5: Observed and modelled mixing ratios at Gadanki. (The left hand y-axis shows value for modelled mixing ratio and right-hand axis shows value for observed mixing ratios)**

## 5 Conclusions and Outlook

The GOSAT and OCO-2 satellites provide global coverage of columnar mixing ratios of CO<sub>2</sub> and CH<sub>4</sub> every 3 and 15 days, respectively. These data are crucial for deriving regional greenhouse gas emission fluxes. However, the accuracy of the derived emission fluxes strongly depends on the precision and accuracy of the satellite products. In our study, we compared GOSAT and OCO-2 satellite-measured columnar mixing ratios of CO<sub>2</sub> and CH<sub>4</sub> with ground-based FTS measurements from a location in South India.

The biases in methane mixing ratios estimated using the GOSAT satellite ranged from  $-9$  to  $-0.6$  ppb, depending on the product and matching criteria used for the collocation of ground and satellite footprints. Even though NIES and UoL XCH<sub>4</sub> dry-air mole fraction derived from same satellite (GOSAT), UoL XCH<sub>4</sub> data has much smaller biases for corresponding spatial box-sizes. These biases in UoL XCH<sub>4</sub> meet ESA's CCI requirement for systematic errors ( $< 10$  ppb) for all the matching criteria, NIES XCH<sub>4</sub> meet the requirement only for intermediate ~~the smallest~~ longitude-latitude box size. However, the bias is marginally higher than the acceptable limit for the middle box-size and does not meet the requirement for the largest box size ( $\pm 30^\circ$  longitude  $\times$   $\pm 10^\circ$  latitude) used for matching ground and satellite pairs.

Again, NIES XCO<sub>2</sub> and ACOS XCO<sub>2</sub> products are derived from same satellite (GOSAT), NIES XCO<sub>2</sub> product does not meet the CCI's systematic error requirement of  $< 0.5$  ppm, whereas ACOS XCO<sub>2</sub> data product not only met the CCI's systematic error requirement, it had ~~The biases in carbon dioxide mixing ratios were the~~ lowest biases for the ACOS v9.2 dataset among the three XCO<sub>2</sub> datasets evaluated. Both the ACOS and OCO-2 data meet ESA's CCI requirement for CO<sub>2</sub> biases ( $< 0.5$  ppm), while the GOSAT-NIES XCO<sub>2</sub> v3.05 values showed higher biases, ranging from 0.644 ppm to 0.983 ppm. The precision requirement of  $< 8$  ppm for XCO<sub>2</sub> set by ESA CCI was met by all three datasets with a significant margin, with scatter values ranging from 0.776 ppm to 1.88 ppm.

~~Our study demonstrates that satellite-based greenhouse gas estimates over South Asia show promising accuracy and precision for emission flux retrievals. In recent years, several new satellites from both public and private organizations have been launched to provide greenhouse gas estimates. This highlights the need for sustained efforts to establish a wider and denser network of Fourier Transform Spectrometer (FTS) across South Asia, which can be used for satellite and model validations with implication for better assessment of GHGs emissions and improved climate modelling. We used to model~~

to understand seasonal changes resulting from local and regional emissions in methane mixing ratios and sectoral composition of the sources. The model captures the overall seasonal variation in methane enhancements—showing peaks during certain months (e.g., November) and lows during others (e.g., June–July). Agriculture sector is contributing about 55% on average, followed by sectors such as waste and wetlands. When comparing the model estimated season variability ( $\Delta\text{XCH}_4$ , which represent only the contribution from emissions in the preceding 10 days) with the observed seasonal changes in the total columnar mixing ratios, the model tends to exhibit a much narrower range of variability. For example, over a given period, the observations show a change of about 100 ppb, while the model shows only around a 20 ppb change. This discrepancy suggests that there are significant changes in background methane mixing ratios with season which might limit use of inverse modelling techniques to estimate emission fluxes. Overall, our study demonstrates that satellite-based greenhouse gas estimates over South Asia show promising accuracy and precision for emission flux retrievals. In recent years, several new satellites from both public and private organizations have been launched to provide greenhouse gas estimates. This highlights the need for sustained efforts to establish a wider and denser network of Fourier Transform Spectrometer (FTS) across South Asia, which can be used for satellite and model validations with implication for better assessment of GHGs emissions and improved climate modelling.

#### **Code availability**

PROFFAST Code used to retrieve columnar concentration of GHGs from raw interferograms is publicly available. The link is provided in the main text as well as in acknowledgement section. Source code of FLEXPART model is publicly available. The link for FLEXPART is provided in the main text and in the acknowledgement section.

#### **Data availability**

Satellite data are publicly available and their links are provided in main text as well as in acknowledgement. Data of ground-based Fourier transform spectrometer will be made available through institute's website or through public repository soon. Currently, they can be obtained by writing email to HG.

#### **Author contribution**

HG, AJ, and FH conceptualised the study. HG, CJ, MS and MF did data curation. HG carried out formal analysis. HG and AA carried out model runs and analysis of model output. HG prepared visualization and wrote original draft. SR, CJ, AJ and FH reviewed and edited the draft.

#### **Competing interests**

One of the authors is a member of the editorial board of journal Atmospheric Measurement and Techniques.



## 534 Acknowledgements

535 Authors gratefully acknowledges following dataset and software providers and their funding agencies. Physical Research  
536 Laboratory is supported by the Department of Space, Government of India. The ERA-Interim reanalysis dataset, Copernicus  
537 Climate Change Service (C3S) available from <https://www.ecmwf.int/en/forecasts/dataset/ecmwf-reanalysis-interim> were used to run FLEXPART model (ECMWF, 2011), A priori profiles of pressure, temperature and species were  
538 obtained from CalTechFtp Server (<https://tcon-wiki.caltech.edu/Main/ObtainingGinputData>). GOSAT satellite data  
539 were obtained from NIES website <http://www.gosat.nies.go.jp/>. OCO-2 satellite data used in this study were produced by  
540 the OCO-2 project at the Jet Propulsion Laboratory, California Institute of Technology, and obtained from the OCO-2  
541 data archive maintained at the NASA Goddard Earth Science Data and Information Services Center (OCO-2 Science  
542 Team, 2019). Source code of FLEXPART model was obtained from <https://www.flexpart.eu>. ECLIPSEv6b inventory  
543 data were provided by International Institute of Applied System Analysis through its website (<https://iiasa.ac.at/models-tools-data/global-emission-fields-of-air-pollutants-and-ghgs>). WetCHARTs version 1.0 – wetlands emission inventory  
544 data were provided by Oak Ridge National Laboratory’s Distributed Active Archive Center (ORNL DAAC) through their  
545 web-site (<https://daac.ornl.gov/>). The PROFFAST v2.4 and PROFFASTpylot software are open source software developed  
546 at KIT under framework of ESA’s COCCON-PROCEEDS project. These software are available at <https://www.imk-asf.kit.edu/english/3225.php> and <https://gitlab.eudat.eu/coccon-kit/proffastpylot>. Authors thank Darko Dubravica and  
547 Benedikt Herkommer for help with PROFFAST algorithm.

## 551 References

- 552 Abrams, M. C., Toon, G. C., & Schindler, R. A. (1994). Practical example of the correction of  
553 Fourier-transform spectra for detector nonlinearity. *Appl. Opt.*, 33, 6307–6314.  
554 <https://doi.org/10.1364/AO.33.006307>.
- 555 Alberti, C., Hase, F., Frey, M., Dubravica, D., Blumenstock, T., Dehn, A., et al. (2022a). Improved  
556 calibration procedures for the EM27/SUN spectrometers of the COllaborative Carbon Column  
557 Observing Network (COCCON). *Atmos. Meas. Tech.*, 15, 2433–2451. <https://doi.org/10.5194/amt-15-2433-2022>.
- 558
- 559 Alberti, C., Tu, Q., Hase, F., Makarova, M. V., Gribanov, K., Foka, S. C., Zakharov, V.,  
560 Blumenstock, T., Buchwitz, et al. (2022b), Investigation of spaceborne trace gas products over St  
561 Petersburg and Yekaterinburg, Russia, by using COllaborative Column Carbon Observing Network  
562 (COCCON) observations, *Atmos. Meas. Tech.*, 15, 2199–2229, [https://doi.org/10.5194/amt-15-](https://doi.org/10.5194/amt-15-2199-2022)  
563 [2199-2022](https://doi.org/10.5194/amt-15-2199-2022).
- 564 Amann, M., Bertok, I., Borken-Kleefeld, J., Cofala, J., Heyes, C., Höglund-Isaksson, L., et al.  
565 (2011). Cost-effective control of air quality and greenhouse gases in Europe: Modeling and policy  
566 applications. *Environmental Modelling & Software*, 26, 1489–1501.  
567 <https://doi.org/10.1016/j.envsoft.2011.07.012>

568 Amann, M., J. Borken-Kleefeld, J. Cofala, C. Heyes, Z. Klimont, P. Rafaj, P. Purohit, W. Schöpp,  
569 and W. Winiwarter (2012), Future emissions of air pollutants in Europe – Current legislation  
570 baseline and the scope for further reductions, TSAP Report #1, International Institute for Applied  
571 Systems Analysis, Laxenburg, Austria.

572 Bergamaschi, P., C. Frankenberg, J. Meirink, M. Krol, F. Dentener, T. Wagner, U. Platt, J. Kaplan,  
573 S. Körner, M. Heimann, et al. (2007), Satellite cartography of atmospheric methane from  
574 SCIAMACHY on board ENVISAT: 2. Evaluation based on inverse model simulations, *J. Geophys.*  
575 *Res. Atmos.*, 112, <https://doi.org/10.1029/2006JD007268>.

576 Bergamaschi, P., C. Frankenberg, J. F. Meirink, M. Krol, M. G. Villani, S. Houweling, F. Dentener,  
577 E. J. Dlugokencky, J. B. Miller, L. V. Gatti, A. Engel, and I. Levin (2009), Inverse modeling of  
578 global and regional CH<sub>4</sub> emissions using SCIAMACHY satellite retrievals, *J. Geophys. Res.*, 114,  
579 <https://doi.org/10.1029/2009JD012287>.

580 Bloom, A. A., Exbrayat, J.-F., van der Velde, I. R., Feng, L., & Williams, M. (2016). The decadal  
581 state of the terrestrial carbon cycle: Global retrievals of terrestrial carbon allocation, pools, and  
582 residence times. *Proc. Natl. Acad. Sci. U.S.A.*, 113, 1285–1290.  
583 <https://doi.org/10.1073/pnas.1515160113>.

584 Bloom, A. A., K. W. Bowman, M. Lee, A. J. Turner, R. Schroeder, J. R. Worden, R. Weidner, K. C.  
585 McDonald, and D. J. Jacob (2017a), A global wetland methane emissions and uncertainty dataset  
586 for atmospheric chemical transport models (WetCHARTs version 1.0), *Geosci. Model Dev.*, 10,  
587 2141–2156, <https://doi.org/10.5194/gmd-10-2141-2017>.

588 Bloom, A. A., K. Bowman, M. Lee, A. J. Turner, R. Schroeder, J. R. Worden, R. J. Weidner, K. C.  
589 McDonald, and D. J. Jacob (2017b), CMS: Global 0.5-deg Wetland Methane Emissions and  
590 Uncertainty (WetCHARTs v1.0), *ORNL DAAC*, Oak Ridge, Tennessee, USA,  
591 <https://doi.org/10.3334/ORNLDAAC/1502>.

592 Bousquet, P., B. Ringeval, I. Pison, E. Dlugokencky, E. Brunke, C. Carouge, F. Chevallier, A.  
593 Fortems-Cheiney, C. Frankenberg, D. Hauglustaine, et al. (2010), Source attribution of the changes  
594 in atmospheric methane for 2006–2008, *Atmos. Chem. Phys.*, 10, 27603–27630,  
595 <https://doi.org/10.5194/acp-10-27603-2010>.

596 Buchwitz, M., B. Dils, H. Boesch, D. Brunner, A. Butz, C. Crevoisier, R. Detmers, C. Frankenberg,  
597 O. Hasekamp, W. Hewson, A. Laeng, S. Noël, J. Notholt, R. Parker, M. Reuter, O. Schneising, P.  
598 Somkuti, A.-M. Sundström, and E. D. Wachter (2017), Product validation and intercomparison  
599 report for essential climate variable greenhouse gases for data set climate research data package no.

4, *ESA Climate Change Initiative*, [Online] Available: [http://www.esa-ghg-cci.org/?q=webfm\\_send/352](http://www.esa-ghg-cci.org/?q=webfm_send/352). (last accessed on 1 Feb 2024).

Chandra, N., S. Hayashida, T. Saeki, and P. K. Patra (2017), What controls the seasonal cycle of columnar methane observed by GOSAT over different regions in India?, *Atmos. Chem. Phys.*, 17, 12633–12643, <https://doi.org/10.5194/acp-17-12633-2017>.

Chevallier, F., P. Bergamaschi, S. Houweling, T. van Leeuwen, and P. I. Palmer (2016), User requirements document for the GHG-CCI project of ESA's Climate Change Initiative, *GHG-CCI*, [Online] Available: <http://www.esa-ghg-cci.org>.

Chevallier, F., M. Fisher, P. Peylin, S. Serrar, P. Bousquet, F.-M. Bréon, A. Chédin, and P. Ciais (2005), Inferring CO<sub>2</sub> sources and sinks from satellite observations: Method and application to TOVS data, *J. Geophys. Res. Atmos.*, 110, <https://doi.org/10.1029/2005JD006390>.

Crisp, D., R. M. Atlas, F.-M. Breon, L. R. Brown, J. P. Burrows, P. Ciais, B. J. Connor, S. C. Doney, I. Y. Fung, D. J. Jacob, C. E. Miller, D. O'Brien, S. Pawson, J. T. Randerson, P. Rayner, R. J. Salawitch, S. P. Sander, B. Sen, G. L. Stephens, P. P. Tans, G. C. Toon, P. O. Wennberg, S. C. Wofsy, Y. L. Yung, Z. Kuang, B. Chudasama, G. Sprague, B. Weiss, R. Pollock, D. Kenyon, S. Schroll (2004), The Orbiting Carbon Observatory (OCO) mission, *Adv. Space Res.*, 34, 700–709, <https://doi.org/10.1016/j.asr.2003.08.062>.

Crisp, D., H. R. Pollock, R. Rosenberg, L. Chapsky, R. A. M. Lee, F. A. Oyafulso, C. Frankenberg, C. W. O'Dell, C. J. Bruegge, G. B. Doran, A. Eldering, B. M. Fisher, D. Fu, M. R. Gunson, L. Mandrake, G. B. Osterman, F. M. Schwandner, K. Sun, T. E. Taylor, P. O. Wennberg, and D. Wunch (2017), The on-orbit performance of the Orbiting Carbon Observatory-2 (OCO-2) instrument and its radiometrically calibrated products, *Atmos. Meas. Tech.*, 10, 59–81, <https://doi.org/10.5194/amt-10-59-2017>.

Crisp, D., C. O'Dell, A. Eldering, B. Fisher, F. Oyafulso, V. Payne, et al. (2021), Orbiting carbon observatory (OCO) - 2 Level 2 Full Physics Algorithm Theoretical Basis Document, *Jet Propulsion Laboratory, California Institute of Technology* under contract with NASA, Pasadena, California.

Dee, D. P., S. M. Uppala, A. J. Simmons, P. Berrisford, P. Poli, S. Kobayashi, et al. (2011), The ERA-Interim reanalysis: configuration and performance of the data assimilation system, *Q. J. R. Meteorol. Soc.*, 137(656), 553–597, <https://doi.org/10.1002/qj.828>.

Dietrich, F., Chen, J., Voggenreiter, B., Aigner, P., Nachtigall, N., and Reger, B.: MUCCnet (2021), Munich Urban Carbon Column network, *Atmos. Meas. Tech.*, 14, 1111–1126, <https://doi.org/10.5194/amt-14-1111-2021>.

632 Dunn, R., F. Aldred, N. Gobron, et al. (2022), Global Climate, *Bull. Am. Meteorol. Soc.*, 103(8),  
633 S11–S142, <https://doi.org/10.1175/bams-d-22-0092.1>.

634 European Centre for Medium-range Weather Forecast (ECMWF, 2011): The ERA-Interim  
635 reanalysis dataset, Copernicus Climate Change Service (C3S) (accessed 30 July 2019), available  
636 from <https://www.ecmwf.int/en/forecasts/dataset/ecmwf-reanalysis-interim>.

637 Feld, L., Herkommer, B., Vestner, J., Dubravica, D., Alberti, C., & Hase, F. (2024),  
638 PROFFASTpylot: Running PROFFAST with Python. *Journal of Open Source Software*, 9, 6481,  
639 <https://doi.org/10.21105/joss.06481>.

640 Fiore, A. M., D. J. Jacob, B. D. Field, D. G. Streets, and S. D. Fernandes (2002), Linking ozone  
641 pollution and climate change: The case for controlling methane, *Geophys. Res. Lett.*, 29, 1919,  
642 <https://doi.org/10.1029/2002GL015601>.

643 Fleming, E. L., C. George, D. E. Heard, C. H. Jackman, M. J. Kurylo, W. Mellouki, et al. (2015),  
644 The impact of current CH<sub>4</sub> and N<sub>2</sub>O atmospheric loss process uncertainties on calculated ozone  
645 abundances and trends, *J. Geophys. Res. Atmos.*, 120, 5267 – 5293,  
646 <https://doi.org/10.1002/2014JD022067>.

647 Frausto-Vicencio, I., Heerah, S., Meyer, A. G., Parker, H. A., Dubey, M., and Hopkins, F. M.  
648 (2023), Ground solar absorption observations of total column CO, CO<sub>2</sub>, CH<sub>4</sub>, and aerosol optical  
649 depth from California's Sequoia Lightning Complex Fire: emission factors and modified  
650 combustion efficiency at regional scales, *Atmos. Chem. Phys.*, 23, 4521–4543,  
651 <https://doi.org/10.5194/acp-23-4521-2023>.

652 Frey, M., M. K. Sha, F. Hase, M. Kiel, T. Blumenstock, R. Harig, G. Surawicz, N. M. Deutscher, K.  
653 Shiomi, J. E. Franklin, H. Bösch, J. Chen, M. Grutter, H. Ohyama, Y. Sun, A. Butz, G. Mengistu  
654 Tsidu, D. Ene, D. Wunch, Z. Cao, O. Garcia, M. Ramonet, F. Vogel, and J. Orphal (2019), Building  
655 the COllaborative Carbon Column Observing Network (COCCON): long-term stability and  
656 ensemble performance of the EM27/SUN Fourier transform spectrometer, *Atmos. Meas. Tech.*, 12,  
657 1513–1530, <https://doi.org/10.5194/amt-12-1513-2019>.

658 Gadhavi, H. S., Renuka, K., Kiran, V. R., Jayaraman, A., Stohl, A., Klimont, Z., & Beig, G. (2015).  
659 Evaluation of black carbon emission inventories using a Lagrangian dispersion model –“ a case  
660 study over southern India. *Atmos. Chem. Phys.*, 15, 1447–1461. [https://doi.org/10.5194/acp-15-](https://doi.org/10.5194/acp-15-1447-2015)  
661 [1447-2015](https://doi.org/10.5194/acp-15-1447-2015).

662 GCOS-200 (2016): The global observing system for climate: Implementation needs, *World*  
663 *Meteorological Organization*.

664 Gisi, M., F. Hase, S. Dohe, and T. Blumenstock (2011), Camtracker: a new camera controlled high  
665 precision solar tracker system for FTIR-spectrometers, *Atmos. Meas. Tech.*, 4, 47–54,  
666 <https://doi.org/10.5194/amt-4-47-2011>.

667 Gisi, M., F. Hase, S. Dohe, T. Blumenstock, A. Simon, and A. Keens (2012), XCO<sub>2</sub> measurements  
668 with a tabletop FTS using solar absorption spectroscopy, *Atmos. Meas. Tech.*, 5, 2969–2980,  
669 <https://doi.org/10.5194/amt-5-2969-2012>.

670 Hase, F., T. Blumenstock, and C. Paton-Walsh (1999), Analysis of the instrumental line shape of  
671 high-resolution Fourier transform IR spectrometers with gas cell measurements and new retrieval  
672 software, *Appl. Opt.*, 38, 3417 – 3422, <https://doi.org/10.1364/AO.38.003417>.

673 Hase, F., J. W. Hannigan, M. T. Coffey, A. Goldman, M. Höpfner, N. B. Jones, C. P. Rinsland, and  
674 S. W. Wood (2004), Intercomparison of retrieval codes used for the analysis of high-resolution,  
675 ground-based FTIR measurements, *J. Quant. Spectrosc. Radiat. Transf.*, 87, 25–52,  
676 <https://doi.org/10.1016/j.jqsrt.2003.12.008>.

677 Herkommer, B., Alberti, C., Castracane, P., Chen, J., Dehn, A., Dietrich, F., Deutscher, N. M., Frey,  
678 M. M., et al. (2024), Using a portable FTIR spectrometer to evaluate the consistency of Total  
679 Carbon Column Observing Network (TCCON) measurements on a global scale: the Collaborative  
680 Carbon Column Observing Network (COCCON) travel standard, *Atmos. Meas. Tech.*, 17, 3467–  
681 3494, <https://doi.org/10.5194/amt-17-3467-2024>.

682 Hoglund-Isaksson, L. (2012), Global anthropogenic methane emissions 2005–2030: technical  
683 mitigation potentials and costs, *Atmos. Chem. Phys.*, 12, 9079–9096, [https://doi.org/10.5194/acp-](https://doi.org/10.5194/acp-12-9079-2012)  
684 [12-9079-2012](https://doi.org/10.5194/acp-12-9079-2012).

685 IPCC 2008, 2006 IPCC Guidelines for National Greenhouse Gas Inventories – A primer, Prepared  
686 by the National Greenhouse Gas Inventories Programme, Eggleston H.S., Miwa K., Srivastava N.  
687 and Tanabe K. (eds), IGES, Japan., 20 pp., ISBN 9784887880320.

688 IMK-ASF, K. (2024a, February 28). Data Processing. Retrieved from [https://www.imk-](https://www.imk-asf.kit.edu/english/3225.php)  
689 [asf.kit.edu/english/3225.php](https://www.imk-asf.kit.edu/english/3225.php).

690 IMK-ASF, K. (2024b). PROFFASTpylot v1.3 documentation. Retrieved from [https://www.imk-](https://www.imk-asf.kit.edu/english/4261.php)  
691 [asf.kit.edu/english/4261.php](https://www.imk-asf.kit.edu/english/4261.php).

692 [Jacobs, N., O'Dell, C. W., Taylor, T. E., Logan, T. L., Byrne, B., Kiel, M., et al. \(2024\). The](#)  
693 [importance of digital elevation model accuracy in XCO<sub>2</sub> retrievals: improving the Orbiting Carbon](#)  
694 [Observatory 2 Atmospheric Carbon Observations from Space version 11 retrieval](#)



695 product. *Atmospheric Measurement Techniques*, 17(5), 1375–1401. [https://doi.org/10.5194/amt-17-](https://doi.org/10.5194/amt-17-1375-2024)  
696 1375-2024.

697 Jain, C. D., V. Singh, S. T. Akhil Raj, B. L. Madhavan, and M. V. Ratnam (2021), Local emission  
698 and long-range transport impacts on the CO, CO<sub>2</sub>, and CH<sub>4</sub> concentrations at a tropical rural site,  
699 *Atmos. Environ.*, 254, 118397, <https://doi.org/10.1016/j.atmosenv.2021.118397>.

700 Jayaraman, A., M. V. Ratnam, A. K. Patra, T. N. Rao, S. Sridharan, M. Rajeevan, et al. (2010),  
701 Study of Atmospheric Forcing and Responses (SAFAR) campaign: overview, *Annales Geophysicae*,  
702 28, 89–101, <https://doi.org/10.5194/angeo-28-89-2010>.

703 Kavitha, M., and P. R. Nair (2016), Region-dependent seasonal pattern of methane over Indian  
704 region as observed by SCIAMACHY, *Atmos. Environ.*, 131, 316–325,  
705 <https://doi.org/10.1016/j.atmosenv.2016.02.008>.

706 Keppel-Aleks, G., G. C. Toon, P. O. Wennberg, and N. M. Deutscher (2007), Reducing the impact  
707 of source brightness fluctuations on spectra obtained by Fourier-transform spectrometry, *Appl. Opt.*,  
708 46, 4774–4779, <https://doi.org/10.1364/AO.46.004774>.

709 Klimont, Z., K. Kupiainen, C. Heyes, P. Purohit, J. Cofala, P. Rafaj, J. Borken-Kleefeld, and W.  
710 Schöpp (2017), Global anthropogenic emissions of particulate matter including black carbon,  
711 *Atmos. Chem. Phys.*, 17, 8681–8723, <https://doi.org/10.5194/acp-17-8681-2017>.

712 Laughner, J. L., J. L. Neu, D. Schimel, P. O. Wennberg, K. Barsanti, K. W. Bowman, et al. (2021),  
713 Societal shifts due to COVID-19 reveal large-scale complexities and feedbacks between  
714 atmospheric chemistry and climate change, *Proc. Natl. Acad. Sci. U.S.A.*, 118,  
715 <https://doi.org/10.1073/pnas.2109481118>.

716 Laughner, J. L., G. C. Toon, J. Mendonca, C. Petri, S. Roche, D. Wunch, et al. (2024). The Total  
717 Carbon Column Observing Network’s GGG2020 data version. *Earth System Science Data*, 16(5),  
718 2197–2260. <https://doi.org/10.5194/essd-16-2197-2024>

719 Messerschmidt, J., R. Macatangay, J. Notholt, C. Petri, T. Warneke, and C. Weinzierl (2010), Side  
720 by side measurements of CO<sub>2</sub> by ground-based Fourier transform spectrometry (FTS), *Tellus B:*  
721 *Chem. Phys. Meteorol.*, 62, 749–758, <https://doi.org/10.1111/j.1600-0889.2010.00491.x>.

722 Marsh, D., M. Mills, D. E. Kinnison, and J.-F. Lamarque (2013), Climate change from 1850 to 2005  
723 simulated in CESM1(WACCM), *J. Climate*, 26, 7372–7391, [https://doi.org/10.1175/JCLI-D-12-](https://doi.org/10.1175/JCLI-D-12-00558.1)  
724 [00558.1](https://doi.org/10.1175/JCLI-D-12-00558.1).

725 NCEP (2000), National Centers for Environmental Prediction/National Weather  
726 Service/NOAA/U.S. Department of Commerce., NCEP FNL Operational Model Global

727 Tropospheric Analyses, continuing from July 1999. Research Data Archive at the National Center  
 728 for Atmospheric Research, Computational and Information Systems Laboratory. 2000 (updated  
 729 daily) <https://doi.org/10.5065/D6M043C6>. Accessed on 15 Sep 2017.

730 Noël, S., K. Weigel, K. Bramstedt, A. Rozanov, M. Weber, H. Bovensmann, and J. P. Burrows  
 731 (2018), Water vapour and methane coupling in the stratosphere observed using SCIAMACHY solar  
 732 occultation measurements, *Atmos. Chem. Phys.*, 18, 4463–4476, [https://doi.org/10.5194/acp-18-](https://doi.org/10.5194/acp-18-4463-2018)  
 733 [4463-2018](https://doi.org/10.5194/acp-18-4463-2018).

734 OCO-2 Science Team (2019), OCO-2 Science Team/Michael Gunson, Annmarie Eldering, ACOS  
 735 GOSAT/TANSO-FTS Level 2 Full Physics Standard Product V9r, Greenbelt, MD, USA, Goddard  
 736 Earth Sciences Data and Information Services Center (GES DISC), Accessed on 1 January 2024,  
 737 10.5067/OSGTIL9OV0PN.

738 O'Dell, C. W., A. Eldering, P. O. Wennberg, D. Crisp, M. R. Gunson, B. Fisher, et al. (2018),  
 739 Improved retrievals of carbon dioxide from Orbiting Carbon Observatory-2 with the version 8  
 740 ACOS algorithm, *Atmos. Meas. Tech.*, 11, 6539–6576, <https://doi.org/10.5194/amt-11-6539-2018>.

741 Olsen, K. S., K. Strong, K. A. Walker, C. D. Boone, P. Raspollini, J. Plieninger, et al. (2017),  
 742 Comparison of the GOSAT TANSO-FTS TIR CH<sub>4</sub> volume mixing ratio vertical profiles with those  
 743 measured by ACE-FTS, ESA MIPAS, IMK-IAA MIPAS, and 16 NDACC stations, *Atmos. Meas.*  
 744 *Tech.*, 10, 3697–3718, <https://doi.org/10.5194/amt-10-3697-2017>.

745 Osterman, G., A. Eldering, C. Cheng, C. O'Dell, D. Crisp, C. Frankenberg, and B. Fisher (2017),  
 746 ACOS Level 2 standard product and Lite data product data user's guide, v7.3, 51 pp.

747 Pak, N. M., Hedelius, J. K., Roche, S., Cunningham, L., Baier, B., Sweeney, C., Roehl, C.,  
 748 Laughner, et al. (2023), Using portable low-resolution spectrometers to evaluate Total Carbon  
 749 Column Observing Network (TCCON) biases in North America, *Atmos. Meas. Tech.*, 16, 1239–  
 750 1261, <https://doi.org/10.5194/amt-16-1239-2023>.

751 Pandit, A. K., Gadhavi, H., Ratnam, M. V., Jayaraman, A., Raghunath, K., and Rao, S. V. B. (2014).  
 752 Characteristics of cirrus clouds and tropical tropopause layer: Seasonal variation and long-term  
 753 trends. *J Atmos and Solar-Terrestrial Phys*, 121, 248–256,  
 754 <https://doi.org/10.1016/j.jastp.2014.07.008>

755 Pandit, A. K., H. S. Gadhavi, M. V. Ratnam, K. Raghunath, S. V. B. Rao, and A. Jayaraman (2015),  
 756 Long-term trend analysis and climatology of tropical cirrus clouds using 16 years of lidar data set  
 757 over Southern India, *Atmos. Chem. Phys.*, 15, 13833–13848, [https://doi.org/10.5194/acp-15-13833-](https://doi.org/10.5194/acp-15-13833-2015)  
 758 [2015](https://doi.org/10.5194/acp-15-13833-2015).

759 Parker, R. J., A. Webb, H. Boesch, P. Somkuti, R. Barrio Guillo, A. Di Noia, et al. (2020), A decade  
760 of GOSAT Proxy satellite CH<sub>4</sub> observations, Earth Syst. Sci. Data, 12, 3383–3412,  
761 <https://doi.org/10.5194/essd-12-3383-2020>.

762 Pathakoti, M., D.V., M., A.L., K., K.S., R., Taori, A., Bothale, R. V., & Chauhan, P. (2024),  
763 Temporal variability of atmospheric columnar CO<sub>2</sub>, CH<sub>4</sub>, CO and N<sub>2</sub>O concentrations using ground-  
764 based remote sensing FTIR Spectrometer, *Advances in Space Research*, 73, 4967–4975,  
765 <https://doi.org/10.1016/j.asr.2024.02.028>.

766 Payne, V., A. Chatterjee, R. Rosenberg, M. Kiel, B. Fisher, L. Dang, et al. (2023), Orbiting carbon  
767 observatory-2 & 3 (OCO-2 & OCO-3) Data Product User’s Guide, Operational Level 2 Lite Files,  
768 *Jet Propulsion Laboratory, California Institute of Technology*, Pasadena, California.

769 Pisso, I., E. Sollum, H. Grythe, et al. (2019), The Lagrangian particle dispersion model FLEXPART  
770 version 10.4, *Geosci. Model Dev.*, 12, 4955–4997, <https://doi.org/10.5194/gmd-12-4955-2019>.

771 Renuka, K., H. Gadhavi, A. Jayarman, S. V. B. Lal, M. Naja, and S. V. B. Rao (2014), Study of  
772 ozone and NO<sub>2</sub> over Gadanki - a rural site in South India, *J. Atmos. Chem.*, 71, 95–112,  
773 <https://doi.org/10.1007/s10874-014-9284-y>.

774 Renuka, K., H. Gadhavi, A. Jayaraman, S. V. B. Rao, and S. Lal (2020), Study of mixing ratios of  
775 SO<sub>2</sub> in a tropical rural environment in south India, *J. Earth Syst. Sci.*, 129,  
776 <https://doi.org/10.1007/s12040-020-1366-4>.

777 Rodgers, C. D. (2000), Inverse Methods for Atmospheric Sounding: Theory and Practice, *Series on*  
778 *Atmospheric, Oceanic and Planetary Physics*, World Scientific Publishing Company.

779 Sagar, V. K., Pathakoti, M., D.V., M., K.S., R., M.V.R., S. S., Hase, F., et al. (2022), Ground-based  
780 remote sensing of total columnar CO<sub>2</sub>, CH<sub>4</sub> and CO using EM27/SUN FTIR spectrometer at a  
781 suburban location (Shadnagar) in India and validation of Sentinel-5P/TROPOMI, *IEEE Geoscience*  
782 *and Remote Sensing Letters*, 19, 1–5, <https://doi.org/10.1109/LGRS.2022.3171216>.

783 Schroeder, R., K. C. McDonald, B. D. Chapman, K. Jensen, E. Podest, Z. D. Tessler, et al. (2015),  
784 Development and evaluation of a multi-year fractional surface water data set derived from  
785 active/passive microwave remote sensing data, *Remote Sensing*, 7, 16688–16732,  
786 <https://doi.org/10.3390/rs71215843>.

787 Sepúlveda, E., M. Schneider, F. Hase, O. E. Garcia, A. Gomez-Pelaez, S. Dohe, T. Blumenstock,  
788 and J. C. Guerra (2012), Long-term validation of tropospheric column-averaged CH<sub>4</sub> mole fractions  
789 obtained by mid-infrared ground-based FTIR spectrometry, *Atmos. Meas. Tech.*, 5, 1425–1441,  
790 <https://doi.org/10.5194/amt-5-1425-2012>.

791 [Sha, M. K., Langerock, B., Blavier, J.-F. L., Blumenstock, T., Borsdorff, T., Buschmann, M., et al.](#)  
792 [\(2021\). Validation of methane and carbon monoxide from Sentinel-5 Precursor using TCCON and](#)  
793 [NDACC-IRWG stations. \*Atmos. Meas. Tech.\*, 14\(9\), 6249–6304. \[https://doi.org/10.5194/amt-14-\]\(https://doi.org/10.5194/amt-14-6249-2021\)](#)  
794 [6249-2021.](#)

795 Sha, M., M. de Maziere, J. Notholt, T. Blumenstock, et al. (2020), Intercomparison of low- and  
796 high-resolution infrared spectrometers for ground-based solar remote sensing measurements of total  
797 column concentrations of CO<sub>2</sub>, CH<sub>4</sub> and CO, *Atmos. Meas. Tech.*, 13, 4791–4839,  
798 <https://doi.org/10.5194/amt-13-4791-2020>.

799 [Someya, Y., Yoshida, Y., Ohyama, H., Nomura, S., Kamei, A., Morino, I., et al. \(2023\). Update on](#)  
800 [the GOSAT TANSO-FTS SWIR Level 2 retrieval algorithm. \*Atmospheric Measurement\*](#)  
801 [Techniques, 16\(6\), 1477–1501. <https://doi.org/10.5194/amt-16-1477-2023>.](#)

802 Stohl, A., B. Aamaas, M. Amann, et al. (2015), Evaluating the climate and air quality impacts of  
803 short-lived pollutants, *Atmos. Chem. Phys.*, 15, 10529–10566, [https://doi.org/10.5194/acp-15-](https://doi.org/10.5194/acp-15-10529-2015)  
804 [10529-2015](#).

805 Suman, M. N. S., H. Gadhavi, V. Ravi Kiran, A. Jayaraman, and S. V. B. Rao (2014), Role of coarse  
806 and fine mode aerosols in MODIS AOD retrieval: a case study over southern India, *Atmos. Meas.*  
807 *Tech.*, 7, 907–917, <https://doi.org/10.5194/amt-7-907-2014>.

808 Turner, A. J., C. Frankenberg, and E. A. Kort (2019), Interpreting contemporary trends in  
809 atmospheric methane, *Proc. Natl. Acad. Sci. U.S.A.*, 116, 2805–2813,  
810 <https://doi.org/10.1073/pnas.1814297116>.

811 ~~Wunch, D., G. C. Toon, J. F. Blavier, R. A. Washenfelder, J. Notholt, B. J. Connor, et al. (2011a),~~  
812 ~~The Total Carbon Column Observing Network, *Philos. Trans. R. Soc. A Math. Phys. Eng. Sci.*, 369,~~  
813 ~~2087–2112, <https://doi.org/10.1098/rsta.2010.0240>.~~

814 Wunch, D., P. O. Wennberg, G. Osterman, B. Fisher, B. Naylor, C. M. Roehl, et al. (2017),  
815 Comparisons of the Orbiting Carbon Observatory-2 (OCO-2) XCO<sub>2</sub> measurements with TCCON,  
816 *Atmos. Meas. Tech.*, 10, 2209–2238, <https://doi.org/10.5194/amt-10-2209-2017>.

817 Yokota, T., Yoshida, Y., Eguchi, N., Ota, Y., Tanaka, T., Watanabe, H., and Maksyutov, S. (2009),  
818 Global concentrations of CO<sub>2</sub> and CH<sub>4</sub> retrieved from GOSAT: First preliminary results. *Sola*, 5,  
819 160–163, <https://doi.org/10.2151/sola.2009-041>.